THE JOURNAL OF PHYSICAL CHEMISTRY A
A JOURNAL OF THE AMERICAN CHEMICAL SOCIETY

pubs.acs.org/JPCA

Article

Solid-State NMR $^{19}F-^{1}H-^{15}N$ Correlation Experiments for Resonance Assignment and Distance Measurements of Multifluorinated Proteins

Pu Duan, Aurelio J. Dregni, and Mei Hong*

Cite This: *J. Phys. Chem. A* 2022, 126, 7021−7032

Read Online

ACCESS | Metrics & More | Article Recommendations | Supporting Information

ABSTRACT: Several solid-state NMR techniques have been introduced recently to measure nanometer distances involving ^{19}F, whose high gyromagnetic ratio makes it a potent nuclear spin for structural investigation. These solid-state NMR techniques either use ^{19}F correlation with ^{1}H or ^{13}C to obtain qualitative interatomic contacts or use the rotational-echo double-resonance (REDOR) pulse sequence to measure quantitative distances. However, no NMR technique is yet available for disambiguating $^{1}H-^{19}F$ distances in multiply fluorinated proteins and protein−ligand complexes. Here, we introduce a three-dimensional (3D) $^{19}F-^{15}N-^{1}H$ correlation experiment that resolves the distances of multiple fluorines to their adjacent amide protons. We show that optimal polarization transfer between ^{1}H and ^{19}F spins is achieved using an out-and-back $^{1}H-^{19}F$ REDOR sequence. We demonstrate this 3D correlation experiment on the model protein GB1 and apply it to the multidrug-resistance transporter, EmrE, complexed to a tetrafluorinated substrate. This technique should be useful for resolving and assigning distance constraints in multiply fluorinated proteins, leading to significant savings of time and precious samples compared to producing several singly fluorinated samples. Moreover, the method enables structural determination of protein−ligand complexes for ligands that contain multiple fluorines.

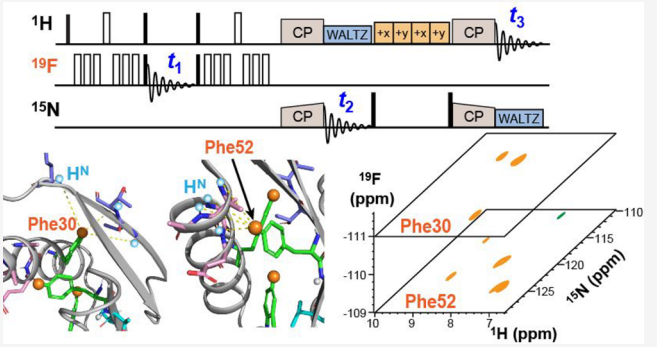

INTRODUCTION

Fluorinated small molecules and fluorinated proteins are ubiquitous in the pharmaceutical industry, medical imaging, and structural biological research. In 2020, ∼25% of all drugs approved by the Food & Drug Administration (FDA) contain fluorine atoms,[1] and this number is estimated to increase to approximately 30%.[2] The incorporation of fluorine in pharmaceutical compounds can improve the metabolism and bioavailability of the drug.[3] Fluorine is also widely incorporated in positron emission tomography (PET) tracers to diagnose cancer, cardiovascular diseases, neurodegenerative disorders, and other diseases.[4−6] While fluorinated small molecules are excellent probes for studying ligand binding to macromolecules, fluorinated proteins provide opportunities for investigating protein structure and dynamics.[7] Although fluorine does not occur naturally in biological macromolecules, it can be readily introduced into proteins biosynthetically or synthetically.[8−10] When sparsely incorporated, fluorine usually causes minimal perturbation to protein structure and function, as can be assessed by ^{13}C, ^{15}N, and ^{1}H NMR and other biophysical techniques.[11,12]

The stable isotope of fluorine, ^{19}F, has many attractive properties for NMR spectroscopy. ^{19}F is a 100% abundant spin-1/2 nucleus with a large gyromagnetic ratio (γ), which is 94% of the γ of ^{1}H. Thus, ^{19}F NMR has intrinsically high detection sensitivity. The ^{19}F chemical shift is extremely sensitive to its electronic environment; hence, it reports on subtle changes in the chemical and conformational structure of the molecule.[13−16] The large ^{19}F γ increases the strength of the dipole−dipole interaction between ^{19}F and other nuclear spins; thus, ^{19}F allows interatomic distances to be measured to longer ranges than currently possible using low-γ nuclei such as ^{13}C and ^{15}N. As a result, ^{19}F has been exploited for distance measurements in magic-angle-spinning (MAS) solid-state NMR spectroscopy for many years.[17,18] However, until recently, the most common approach for this purpose has been one-dimensional (1D) rotational-echo double-resonance (REDOR), which measures one distance at a time, giving low throughput.[19] To accelerate ^{19}F-based distance measurements, multidimensional solid-state NMR techniques that achieve

Received: July 20, 2022
Revised: September 10, 2022
Published: September 23, 2022

Downloaded via MASSACHUSETTS INST OF TECHNOLOGY on October 13, 2022 at 18:47:33 (UTC).
See https://pubs.acs.org/sharingguidelines for options on how to legitimately share published articles.

ACS Publications
© 2022 American Chemical Society

https://doi.org/10.1021/acs.jpca.2c05154
J. Phys. Chem. A 2022, 126, 7021−7032

$^{13}C-^{19}F$, $^{1}H-^{19}F$, and $^{19}F-^{19}F$ correlation and distance measurements have been introduced in the past few years.[7] These techniques operate at relatively high magnetic fields of 11.7 T or above and under relatively fast MAS frequencies of 25−110 kHz. Thus, they have higher sensitivity and resolution than traditional low-field slow-MAS ^{19}F NMR experiments. Two main approaches, heteronuclear correlation (HETCOR) and REDOR, have been explored under these high-field fast-MAS conditions. The HETCOR experiments typically involve cross-polarization (CP) between ^{19}F and other nuclei to assign the resonances and extract qualitative distance information.[20−24] Similarly, homonuclear $^{19}F-^{19}F$ correlation experiments using either spin diffusion[25,26] or dipolar recoupling for polarization transfer have been used, with semiquantitative distances extracted from cross-peak intensities.[27−29] These two-dimensional (2D) heteronuclear and homonuclear correlation experiments have been demonstrated on fluorinated small molecules, pharmaceutical compounds,[30−32] model proteins, and the human immunodeficiency virus (HIV-1) capsid protein.[23,26]

Compared to correlation experiments that use cross peak intensities to derive semi-quantitative distance information, REDOR relies on time-dependent dipolar dephasing to provide quantitative distance constraints between ^{19}F and a heteronuclear spin. To increase the throughput of REDOR NMR, we recently demonstrated a 2D $^{13}C-^{13}C$ spectrally resolved $^{13}C-^{19}F$ REDOR experiment.[21] Similarly, $^{1}H-^{19}F$ REDOR can be conducted in a 2D $^{1}H-^{15}N$ spectrally resolved fashion with ^{1}H detection, thus giving high sensitivity as well as excellent site-specific resolution.[33] These 2D resolved REDOR distance experiments have been applied to several membrane proteins and amyloid proteins for structural studies. These include the transmembrane (TM) domains of the SARS-CoV-2 envelope (E) protein,[34] the influenza BM2 protein,[35,36] the multidrug-resistance transporter EmrE,[37,38] and the Alzheimer's Aβ40 fibril bound to a PET tracer.[39]

For ^{19}F REDOR experiments on singly fluorinated proteins or small molecules, no explicit ^{19}F chemical shift encoding is necessary. However, for multiply fluorinated systems, ^{19}F chemical shift encoding and correlation with other nuclei become important for assigning distance constraints to specific fluorine atoms. The $^{19}F-^{13}C$ and $^{19}F-^{1}H$ 2D HETCOR experiments are often not sufficient to resolve the signals of the residues that are close to each fluorine. Therefore, to better resolve the signals of fluorine-proximal residues, two chemical shift dimensions in addition to ^{19}F are desirable. Since 2D $^{13}C-^{13}C$ correlation experiments have low sensitivity while $^{1}H-^{1}H$ 2D correlation experiments have low chemical-shift dispersion, correlating two different nuclei with ^{19}F is expected to give the highest information content.

In this study, we introduce 2D and three-dimensional (3D) ^{19}F, ^{1}H, and ^{15}N correlation experiments to resolve the signals of fluorine-proximal protein residues. We choose ^{15}N as the third nucleus because $^{1}H-^{15}N$ correlation is now the standard fingerprint among ^{1}H-detected solid-state NMR experiments. We compare several polarization transfer methods to achieve triple-resonance $^{1}H-^{19}F-^{15}N$ correlation. We show that an out-and-back (OaB) REDOR-CP experiment and a Lee−Goldberg cross-polarization (LG-CP) experiment both have adequate sensitivity. We demonstrate these techniques on the model protein GB1 and show that the $^{1}H^{N}$-^{19}F correlation spectra can be disambiguated without the use of multiple ^{13}C, ^{2}H, ^{15}N (CDN)-labeled protein samples. We also apply the OaB REDOR-CP experiment to the multidrug-resistance transporter, EmrE, bound to a multifluorinated substrate. The 3D correlation experiment resolves, for the first time, the specific protein side chains that are in close contact to each fluorine of this tetrafluorinated ligand.

METHODS

Preparation of Deuterated and Fluorinated Microcrystalline GB1. Uniformly CDN-labeled GB1 containing one or two fluorinated residues was expressed, purified, and crystallized using a modified protocol from the literature.[21,40] One sample contains a single 5-^{19}F-Trp43 label (W-GB1), and the second sample contains 4-^{19}F-labeled Phe30 and Phe52 (FF-GB1).

All isotopically labeled reagents were obtained from Cambridge Isotope Laboratories. CDN-labeled and fluorinated GB1 was expressed in M9 minimal media by a stepwise training of the bacteria from protonated culture to deuterated culture and by using glyphosate to introduce the fluorinated amino acids. All growth and expression media contain 100 mg/mL ampicillin.

To express CDN-labeled FF-GB1, a 15 mL Luria broth (LB) starter culture in H_2O was inoculated with ampicillin-resistant *Escherichia coli* stored in a glycerol stock, and the cells were grown at 37 °C for ∼14 h, reaching an OD_{600} of ∼4. About 0.5 mL of this starter culture was added to 12.5 mL of filter-sterilized LB media in D_2O and allowed to grow to an OD_{600} of ∼1.3 in 3 h. This 12.5 mL of LB/D_2O culture was then added to 50 mL of filter-sterilized M9 media, which contains 2 g/L ^{13}C-glucose-d_7 and 1 g/L $^{15}NH_4Cl$ in 99% D_2O. The cells were allowed to grow in the M9 media at 37 °C to reach an OD_{600} of ∼1.0. The culture was then added to 150 mL of M9/D_2O media to a volume of 220 mL and grew for another hour. At this point, 25 mg each of L-tyrosine, L-tryptophan, and 4-^{19}F-phenylanaline were dissolved in 5 mL of D_2O as the aromatic amino acid solution. When the M9/D_2O media reached an OD_{600} of ∼0.7, glyphosate was added to a final concentration of 1 g/L to suspend the aromatic amino acid synthesis in the cells. After 5 min of incubation at room temperature, the aromatic amino acid solution was added to the culture. The cells were grown for another 2 h to an OD_{600} of ∼1.0, and then another 1 g/L of ^{13}C-glucose-d_7 was added together with 30 mg of isopropyl β-d-1-thiogalactopyranoside (IPTG) to start protein expression. The total concentration of the ^{13}C-labeled glucose was 3 g/L. GB1 expression proceeded for 4 h at 37 °C, and then the cells were harvested by centrifugation at 5000*g*. The cell pellet was resuspended in 40 mL of lysis buffer containing 50 mM potassium phosphate and 200 mL of sodium chloride at pH 7. The cells were lysed using sonication on ice for 10 min. The lysate was centrifuged at 16 000*g* for 1 h, and the protein in the supernatant was purified by size-exclusion chromatography.[21] CDN-labeled W-GB1 was expressed and purified similarly, except that L-phenylalanine, L-tyrosine, and 5-^{19}F-tryptophan were used in the aromatic amino acid solution.

To assess the purity and ^{19}F incorporation levels of the protein, matrix-assisted laser desorption/ionization time-of-flight (MALDI-TOF) mass spectra were measured for CDN W-GB1, CDN FF-GB1, natural abundance GB1, natural abundance W-GB1, and natural abundance lysozyme C (Figure S1). The molecular weight difference between the

https://doi.org/10.1021/acs.jpca.2c05154
J. Phys. Chem. A 2022, 126, 7021−7032

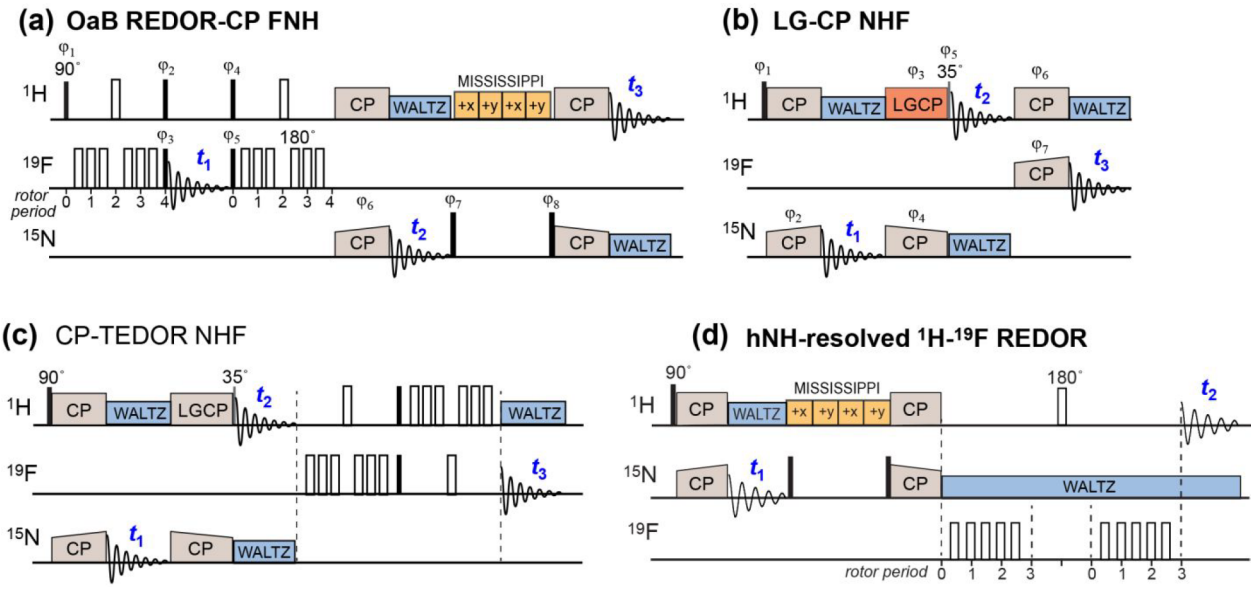

Figure 1. Pulse diagrams for correlating ^{1}H, ^{15}N, and ^{19}F chemical shifts and for ^{1}H−^{19}F distance measurements. The 3D experiments are named in the order of chemical shift encoding. (a) The OaB REDOR-CP FNH experiment. (b) The LG-CP NHF experiment. The crucial spin-diffusion free LG spin lock on ^{1}H is colored in red. (c) The CP-TEDOR NHF experiment. This scheme does not work well due to fast relaxation of the multi-spin ^{19}F−^{1}H coherence. (d) The 2D hNH-resolved ^{1}H−^{19}F REDOR experiment. (Adapted with permission from ref 33. Copyright 2019 American Chemical Society.) Phase cycles (ϕ_i) for the pulse sequences in (a, b) are given in the Methods section. Full Bruker pulse programs for (a, b) are provided in the Supporting Information.

unlabeled GB1 and unlabeled 5-^{19}F-Trp43 GB1 and between W-GB1 and FF-GB1 suggests that both fluorinated proteins have more than 90% ^{19}F incorporation.

To produce microcrystals, W-GB1 and FF-GB1 were dialyzed against 50 mM potassium phosphate at pH 5.5 in 100% H_2O for 32 h (outer solution changed every 8 h) and concentrated to 30 mg/mL, as estimated by A_{280}. The protein was mixed with isopropanol and 2-methyl-2,4-pentanediol at a 1:1:2 volume ratio and incubated at 4 °C overnight.[41] About 8 mg (dry mass) of CDN FF-GB1 and 4 mg of CDN W-GB1 were crystallized. The hydrated microcrystals were packed into 1.9 mm Bruker MAS rotors by centrifugation (3000*g*) using a Beckman Coulter Allegra X-15R centrifuge with a swinging bucket rotor. In addition, microcrystals containing ∼2 mg of CDN FF-GB1 were centrifuged (311,000*g*) into a 1.3 mm Bruker rotor using a Beckman Optima XL-80 centrifuge with an SW60 Ti rotor.

CDN-labeled S64 V-EmrE was expressed and purified as described previously.[38] The protein was bound to DMPC-d_{54} (DMPC = dimyristoylphosphatidylcholine) bilayers at pH 8.0. The sample was incubated with an excess amount of the fluorinated substrate 4-^{19}F-tetraphenylphosphonium (F_4-TPP$^+$) at room temperature with end-to-end rocking for more than 16 h. Excess F_4-TPP$^+$ was removed using microcentrifugation (7500*g*, 5 min).

Solid-State NMR Experiments. All solid-state NMR experiments were conducted on a 14.1 T Bruker Avance III HD NMR spectrometer operating at ^{1}H, ^{19}F, and ^{15}N Larmor frequencies of 600.10, 564.66, and 60.81 MHz. The ^{19}F-containing pulse sequences were implemented on a Bruker 1.9 mm HFX MAS probe. The samples were spun at 38 kHz at a thermocouple-recorded temperature of 273 K. At this spinning rate, frictional heating increases the sample temperature by ∼25 K, giving a sample temperature of ∼298 K. The temperature differential was estimated by measuring the water ^{1}H chemical shift of hydrated protein samples spinning under similar conditions using the equation T_{eff} (K) = 96.9 × (7.83 − δ_{H_2O}).[42] The ^{1}H chemical shift was externally referenced to sodium trimethylsilyl-propanesulfonate (DSS) at 0 ppm. The ^{15}N chemical shift was externally referenced to the Phe amide signal of the tripeptide Met-Leu-Phe (formyl-MLF) at 110.09 ppm on the liquid ammonia scale.[43] The ^{19}F chemical shift was referenced to the ^{19}F peak of crystalline 5-^{19}F-tryptophan at −122.10 ppm on the CF_3Cl scale. ^{1}H and ^{15}N chemical shifts of FF-GB1 were assigned using the 3D hCANH experiment under 55 kHz MAS on a 1.3 mm HXY probe. The thermocouple temperature was 253 K, and the actual sample temperature was ∼290 K. The ^{13}C chemical shift was referenced to the 14.0 ppm methyl ^{13}C peak of Met in formyl-MLF on the tetramethylsilane (TMS) scale.

Typical radiofrequency (RF) field strengths for excitation and refocusing were 83.3 kHz on ^{1}H, 50 kHz on ^{15}N, 62.5 kHz on ^{13}C, and 71.4 kHz on ^{19}F. WALTZ-16 decoupling at an RF field strength of 10 kHz was applied on the ^{1}H, ^{15}N, and ^{13}C channels for all experiments shown in Figure 1. Solvent suppression in the ^{1}H-detected hNH, FNH, and hCANH experiments was achieved using the MISSISSIPPI sequence at an RF field strength of 15 kHz on the ^{1}H channel.[44] More detailed experimental conditions are listed in Table S1.

The pulse sequences for the 3D OaB REDOR-CP FNH and the 3D LG-CP NHF are provided in the Supporting Information. Phase cycles for the 3D OaB REDOR-CP FNH experiment (Figure 1a) are Φ_1 = 13, Φ_2 = 8 × (0) 8 × (2), Φ_3 = 0, Φ_4 = 2, Φ_5 = 22 00, Φ_6 = 1, Φ_7 = 0, Φ_8 = 0000 2222, and $\Phi_{rec'r}$ = 1331 3113 3113 1331. Here, 0, 1, 2, and 3 correspond to +*x*, +*y*, −*x*, and −*y*, respectively. The ^{19}F 180° pulses in the REDOR pulse train were phase-incremented using XY-16.[45] It is worth noting that the two-step phase cycling (Φ_2) of the 90° ^{1}H storage pulse is necessary to prevent the ^{1}H diagonal artifacts due to imperfect ^{1}H inversion pulses. Phase cycles for the 3D LG-CP NHF experiment (Figure 1b) are Φ_1 = 13, Φ_2

https://doi.org/10.1021/acs.jpca.2c05154
J. Phys. Chem. A 2022, 126, 7021−7032

= Φ_3 = 1, Φ_4 = 11 33, Φ_5 = 0, Φ_6 = 1111 3333, Φ_7 = 1, and $\Phi_{rec'r}$ = 1331 3113. No phase cycling is implemented on the ^{1}H 180° pulses in the REDOR period.

All NMR spectra were processed in the Bruker Topspin software, using versions 3.2, 3.5, and 4.1. Version 3.2 allow visualization of 1D cross sections of the 2D planes of 3D correlation spectra and allows direct overlay of 2D planes of 3D spectra with measured 2D spectra. Thus, we have found it to be superior to the newer Topspin versions for spectral analysis.

RESULTS

Design of ^{1}H−^{15}N−^{19}F Correlation NMR Experiments.

To design a high-sensitivity 3D experiment that correlates ^{1}H, ^{19}F, and ^{15}N chemical shifts, we consider two main factors: the detection nucleus and the polarization transfer method between ^{1}H and ^{19}F spins. Either ^{1}H or ^{19}F can serve as a high-sensitivity detection spin, giving two possibilities for pulse sequence design. Polarization transfer between ^{1}H and ^{15}N can be readily achieved by CP. Thus, the only remaining design variable is the ^{1}H−^{19}F polarization transfer method, which can be either a REDOR-based pulse sequence or CP. Within the various implementations of REDOR, we can use OaB REDOR,[43] in which antiphase magnetization is created, rotated to antiphase coherence of the second spin to encode chemical shift evolution, and then rotated back and refocused on the initial spin. Alternatively, one can implement TEDOR,[46] in which the antiphase coherence is rotated to and then refocused on the second spin, achieving complete magnetization transfer. Due to the sparseness of the ^{19}F dimension and the ability to reduce the number of CP steps, the OaB REDOR experiment is best detected using proton. Therefore we appended the hNH sequence after the REDOR module to form a 3D FNH experiment. The CP and TEDOR based experiments can be detected with either ^{19}F or ^{1}H. To avoid water suppression and to minimize the number of polarization transfer steps, we implemented both as ^{19}F-detected experiments. Figure 1a−c shows three of the four pulse diagrams tested based on these considerations. The experiments are named in the order of the chemical shift encoding of the three frequency dimensions, preceded by the method of coherence transfer. The OaB REDOR-CP FNH experiment (Figure 1a) is the only pulse sequence with ^{1}H detection. Among the three ^{19}F-detected experiments, the CP-TEDOR NHF experiment uses CP for ^{15}N−^{1}H polarization transfer and TEDOR for ^{1}H−^{19}F polarization transfer (Figure 1c). The LG-CP NHF experiment uses LG spin lock on the ^{1}H channel[47] to achieve spin-diffusion free polarization transfer from ^{15}N to ^{1}H and then uses regular CP for ^{1}H to ^{19}F polarization transfer (Figure 1b). The CP NHF experiment differs from the LG-CP NHF experiment only in that regular CP is used for ^{15}N−^{1}H polarization transfer; thus, its pulse diagram is not shown. The presence or absence of ^{1}H spin diffusion during the ^{15}N−^{1}H polarization transfer is a crucial detail, and CP NHF is not tenable for ^{19}F−^{15}N−^{1}H correlation. For comparison, we also show the previously published 2D hNH resolved ^{1}H−^{19}F pulse sequence (Figure 1d) for long-range distance measurements.[33]

We first compare the OaB REDOR-CP FNH and CP-TEDOR NHF experiments. The former evolves antiphase ^{19}F−^{1}H magnetization during the ^{19}F chemical shift evolution period and then converts it to ^{1}H single-quantum magnetization for CP to ^{15}N. ^{15}N chemical shift evolution during t_2 is followed by a reverse CP to amide protons for detection. The OaB ^{1}H−^{19}F polarization transfer block is similar to the transfer element in the ZF-TEDOR experiment for ^{13}C−^{15}N correlation;[48] however, it is important to note that no z-filters are used here in order to avoid ^{1}H spin diffusion. In comparison, the CP-TEDOR NHF experiment transfers the ^{15}N-encoded amide ^{1}H magnetization to ^{19}F using the TEDOR element. We show below that these two methods of ^{1}H−^{19}F coherence transfer have different spin dynamics when multiple protons are coupled to each fluorine.

We consider a three-spin system containing two protons, ^{1}H$_1$, ^{1}H$_2$, and a single ^{19}F. We assume the ^{1}H$_1$-^{19}F distance is much shorter than the ^{1}H$_2$-^{19}F distance, so that the ^{1}H$_1$-^{19}F dipolar coupling $\omega_{d,1}$ is much stronger than the ^{1}H$_2$-^{19}F dipolar coupling $\omega_{d,2}$. This situation is expected for most samples of interest, whether the fluorine is incorporated into protein side chains or in a small molecule. The closest protons usually occur in the fluorine-containing residue or small molecule, which is usually undeuterated, while the more remote protons can be an amide proton in a CDN-labeled protein.

In the OaB REDOR-CP experiment, the transverse magnetization $H_{1x} + H_{2x}$ of the two protons is converted to ^{1}H antiphase magnetization with ^{19}F by the average REDOR Hamiltonian $\bar{\omega}_{d,1}\, 2H_{1z}\, F_z + \bar{\omega}_{d,2}\, 2H_{2z}\, F_z$ during the REDOR mixing time t_m.

$$H_{1x} + H_{2x} \xrightarrow{t_m} H_{1x}\cos\bar{\omega}_{d,1}t_m - 2H_{1y}F_z\sin\bar{\omega}_{d,1}t_m + H_{2x}\cos\bar{\omega}_{d,2}t_m - 2H_{2y}F_z\sin\bar{\omega}_{d,2}t_m \quad (1)$$

Here, $\bar{\omega}_{d,1}$ and $\bar{\omega}_{d,2}$ are the time-averaged dipolar couplings under the REDOR pulse sequence.[19,49] We neglect the cosine terms, as they lack ^{19}F correlation and are filtered out by phase cycling. The pair of 90° pulses on ^{1}H and ^{19}F converts the sine terms from ^{1}H antiphase magnetization to ^{19}F antiphase magnetization $2H_{1z}F_y \sin\bar{\omega}_{d,1}t_m + 2H_{2z}F_y \sin\bar{\omega}_{d,2}t_m$. The ensuing ^{19}F chemical shift evolution modulates this ^{19}F antiphase magnetization by a factor $e^{-i\Omega_F t_1}$, after which the second pair of 90° ^{1}H and ^{19}F pulses reconverts the ^{19}F antiphase magnetization back to ^{1}H antiphase magnetization.

$$\xrightarrow{90°\text{pulses}} (2H_{1y}F_z\sin\bar{\omega}_{d,1}t_m + 2H_{2y}F_z\sin\bar{\omega}_{d,2}t_m)e^{-i\Omega_F t_1} \quad (2)$$

During the second half of the REDOR mixing time, each term of the ^{1}H antiphase magnetization evolves under its respective dipolar coupling, $\bar{\omega}_{d,1}2H_{1z}F_z$ or $\bar{\omega}_{d,2}2H_{2z}F_z$, into observable ^{1}H single-quantum coherence (again neglecting cosine terms that are removed by phase cycling).

$$\xrightarrow{t_m} (H_{1x}\sin^2\bar{\omega}_{d,1}t_m + H_{2x}\sin^2\bar{\omega}_{d,2}t_m)e^{-i\Omega_F t_1} \quad (3)$$

Therefore, each proton's magnetization is modulated by the fluorine chemical shift, as desired, and is scaled by each proton's effective transfer efficiency, $\sin^2\bar{\omega}_{d,i}t_m$. This transfer efficiency is independent of the other proton's interactions with the fluorine.

The TEDOR sequence begins similarly, with an initial REDOR block followed by a pair of 90° pulses on the ^{1}H and ^{19}F channels. Again, these steps convert ^{1}H magnetization to ^{19}F antiphase magnetization. The conversion can be written as follows.

https://doi.org/10.1021/acs.jpca.2c05154
J. Phys. Chem. A 2022, 126, 7021−7032

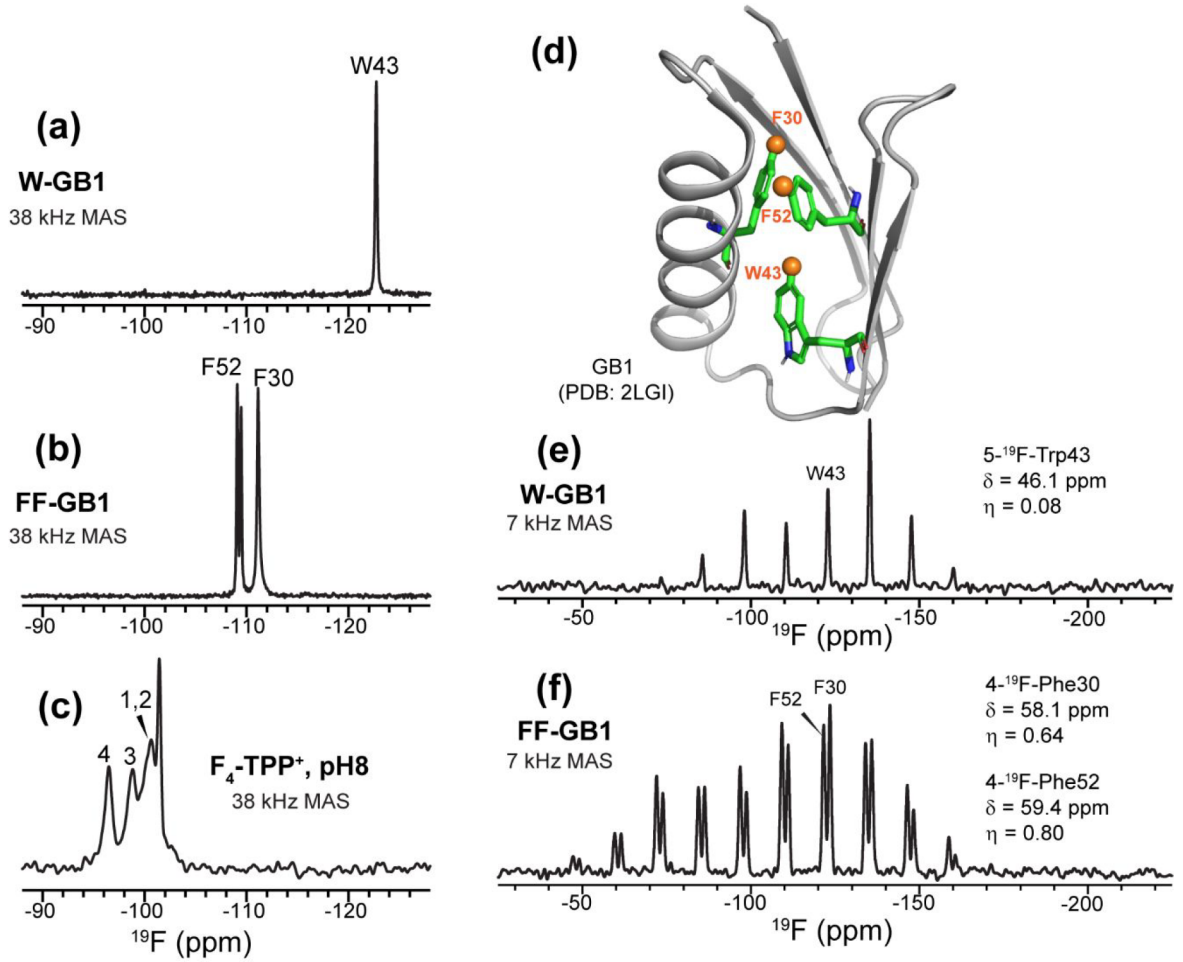

Figure 2. 1D ^{19}F DP spectra of fluorinated GB1 and F_4-TPP$^+$ bound EmrE in lipid bilayers. Spectra in (a–c) were measured under 38 kHz MAS, while spectra in (e, f) were measured under 7 kHz MAS. (a) ^{19}F spectrum of 5-^{19}F-Trp43 labeled GB1, measured with a recycle delay of 5.5 s. The Trp43 ^{19}F T_1 relaxation time is 4.0 s. (b) ^{19}F spectrum of 4-^{19}F-Phe labeled GB1, measured with a recycle delay of 25 s. The ^{19}F T_1 relaxation times are 3.7 s for F52 and 10.7 s for F30. (c) ^{19}F spectrum of F_4-TPP$^+$ bound to EmrE, measured with a recycle delay of 2 s. (d) Structure of GB1, showing the positions of 4-^{19}F-Phe30, 4-^{19}F-Phe52, and 5-^{19}F-Trp43. (e) ^{19}F DP spectrum FF-GB1 under 7 kHz MAS. Fitting the spinning sideband intensities yielded the ^{19}F anisotropy parameter δ and asymmetry parameter η. (b) ^{19}F DP spectrum of W-GB1 under 7 kHz MAS. Fitting the spinning sideband intensities yielded the ^{19}F CSA parameters.

$$H_{1x} + H_{2x} \xrightarrow{t_m} -2H_{1y}F_z \sin \bar{\omega}_{d,1}t_m - 2H_{2y}F_z \sin \bar{\omega}_{d,2}t_m \xrightarrow{90^\circ \text{ pulses}} 2H_{1z}F_y \sin \bar{\omega}_{d,1}t_m + 2H_{2z}F_y \sin \bar{\omega}_{d,2}t_m \quad (4)$$

However, unlike OaB REDOR, in the second half of the TEDOR mixing period, each of the ^{19}F antiphase magnetization terms will be influenced by dipolar couplings to both ^{1}H spins, $\bar{\omega}_{d,1}2H_{1z}F_z + \bar{\omega}_{d,2}2H_{2z}F_z$. Sequential evolution by the two commuting dipolar couplings gives rise to observable ^{19}F magnetization that is modulated by the product of sine and cosine terms of the two dipolar phases.

$$\xrightarrow{t_m} F_x \sin^2 \bar{\omega}_{d,1}t_m \cos \bar{\omega}_{d,2}t_m + F_x \sin^2 \bar{\omega}_{d,2}t_m \cos \bar{\omega}_{d,1}t_m \quad (5)$$

Importantly, the transfer efficiency of each proton spin i to the fluorine not only depends on its own coupling to the fluorine $\sin^2 \bar{\omega}_{d,i}t_m$ but also depends on a factor $\cos \bar{\omega}_{d,j}t_m$ for every other proton j coupled to the fluorine. The cosine terms reduce the magnitude of the observable ^{19}F magnetization, especially because mixing times that maximize the $\sin^2 \bar{\omega}_{d,i}t_m$ terms will generally produce low values of $\cos \bar{\omega}_{d,j}t_m$. If the second mixing period t_{m2} is chosen to be different from the first mixing period t_{m1} before the 90° pulses, then the modulation terms become $\sin \bar{\omega}_{d,1}t_{m1} \sin \bar{\omega}_{d,1}t_{m2} \cos \bar{\omega}_{d,2}t_{m2}$ and $\sin \bar{\omega}_{d,2}t_{m1} \sin \bar{\omega}_{d,2}t_{m2} \cos \bar{\omega}_{d,i}t_{m2}$, but these are still smaller than the optimal efficiency of $\sin^2 \bar{\omega}_{d,i}t_m$ for the OaB REDOR experiment.

This density operator analysis indicates that, for all realistic situations where multiple protons are coupled to each fluorine, the OaB REDOR-CP experiment should have higher sensitivity than the CP-TEDOR experiment. Indeed, this is confirmed experimentally by the GB1 data below (Figure S3a). Based on similar arguments, we expect that OaB REDOR from ^{19}F to ^{1}H would have even worse sensitivity, as both REDOR periods would experience multiple couplings.

Cross-polarization between ^{1}H and ^{19}F is used in the LG-CP NHF experiment (Figure 1b) as well as the CP NHF experiment (pulse diagram not shown). Between these two, the LG-CP experiment is expected to have higher sensitivity because the fluorinated residues or small molecules are usually undeuterated. The resulting ^{1}H spin diffusion, when not suppressed during CP, is expected to lead to ^{15}N–^{1}H correlations not only for directly bonded amides but also

https://doi.org/10.1021/acs.jpca.2c05154
J. Phys. Chem. A 2022, 126, 7021–7032

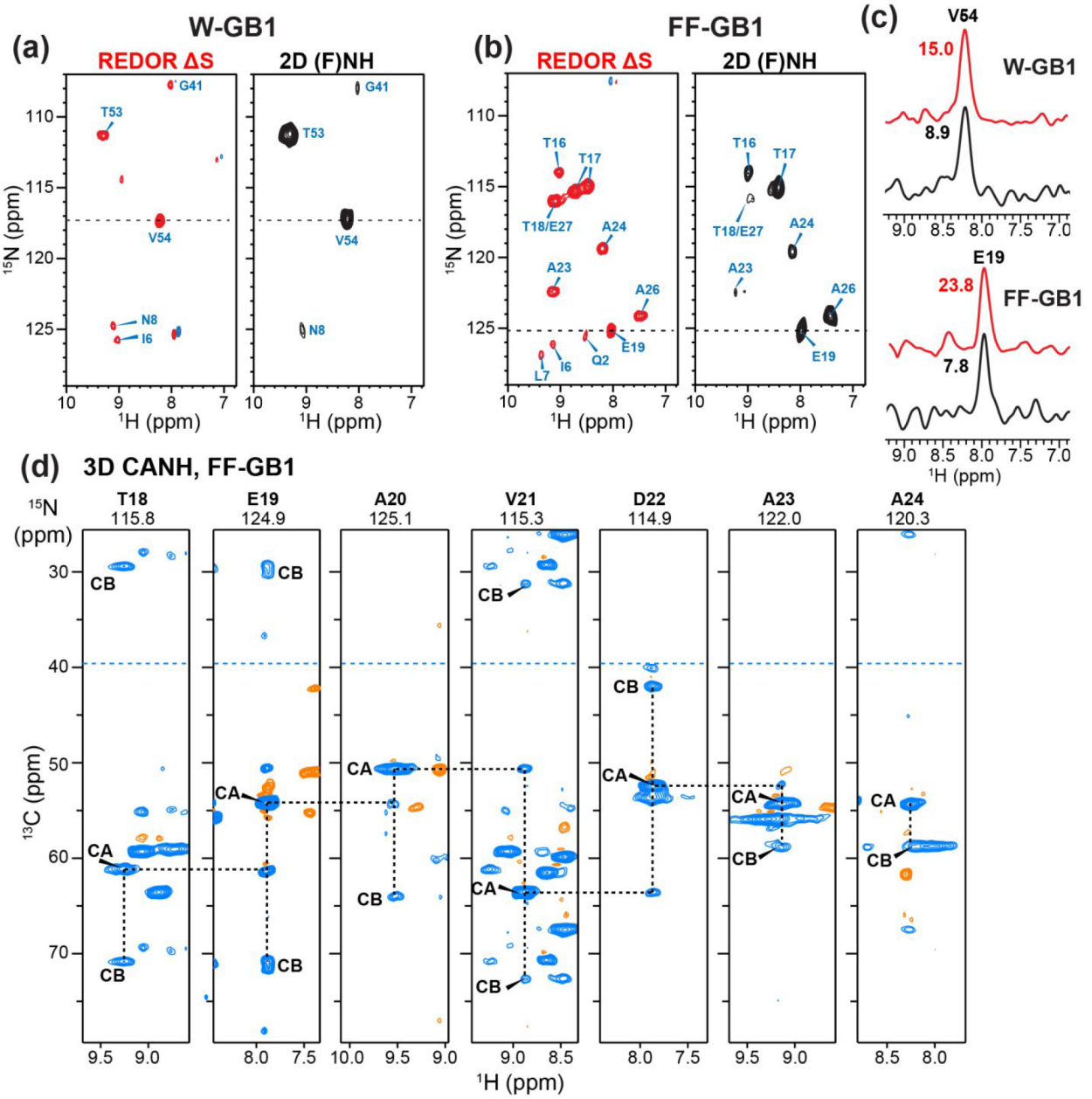

Figure 3. Comparison of 2D hNH-resolved $^{1}H-^{19}F$ REDOR difference spectrum (red) and 2D OaB REDOR-CP (F)NH correlation spectrum (black) of fluorinated GB1. (a) Spectra of FF-GB1. The REDOR ΔS spectrum was measured with a mixing time of 1.89 ms, while the OaB REDOR-CP (F)NH spectrum was measured with a $^{1}H-^{19}F$ mixing time of 2 × 1.1 ms. All strong difference signals in the REDOR ΔS spectrum are also detected in the (F)NH spectrum. (b) Spectra of W-GB1, measured using the same REDOR mixing times as in (a). ^{1}H and ^{15}N chemical shift assignment was taken from a previous study.[33] (c) Representative 1D cross sections of the REDOR ΔS spectra and (F)NH spectra to compare the SNRs of the two experiments. The SNRs of V54 and E19 are indicated. For this sensitivity comparison, the 1D cross sections are processed with the same Gaussian window function (LB = −15, GB = 0.07) for the REDOR and (F)NH spectra, while the 2D spectra shown in (a, b) are processed using slightly different window functions. (d) Representative ^{13}CA-$^{1}H^{N}$ planes of the 3D hCANH spectrum of CDN-labeled FF-GB1. Positive and negative intensities are represented by blue and orange contours. Cross peaks within each residue are connected by vertical dashed lines in each strip, while sequential cross peaks are connected by horizontal dashed lines between strips. Blue dashed lines at ∼40 ppm in the ^{13}C dimension mark the boundary of the ^{13}C dimension above which peaks are aliased. Chemical shifts assignment is guided by literature values.[53,54]

between aromatic protons and the ^{15}N, complicating spectral analysis (Figure S3b). Lee−Goldberg CP suppresses this ^{1}H spin diffusion,[47,50] thus ensuring the detection of one-bond $^{15}N-^{1}H$ cross peaks for those amide protons that are in close proximity to the fluorines.

^{1}H, ^{15}N, and ^{19}F Correlation Spectra of Fluorinated GB1. We assessed the ^{19}F incorporation and ^{19}F chemical shifts of fluorinated GB1 and substrate-bound EmrE using MALDI-MS and 1D ^{19}F direct-polarization (DP) experiments. The mass spectra of unlabeled GB1, fluorinated GB1, and CDN-labeled and fluorinated GB1 samples show a dominant peak whose masses differ in accordance with the presence of one or two fluorines at a greater than 90% level in the protein (Figure S1a−f). The two fluorinated GB1 samples are highly pure, as assessed by the size-exclusion chromatographs (Figure S1g).

https://doi.org/10.1021/acs.jpca.2c05154
J. Phys. Chem. A 2022, 126, 7021−7032

1D ^{19}F DP spectra were measured under 38 kHz MAS to give the isotropic chemical shifts and under 7 kHz to give spinning sideband intensities (Figure 2). The singly fluorinated W-GB1 exhibits a narrow ^{19}F peak at −122.7 ppm (Figure 2a), consistent with previous data.[21] The 2D hNH fingerprint spectrum of this W-GB1 sample shows a single set of ^{15}N−H^{N} correlation peaks, indicating high structural homogeneity. The doubly fluorinated FF-GB1 sample exhibits three peaks in the quantitative ^{19}F DP spectra: a pair of peaks at −109.1 and −109.5 ppm and an isolated peak at −111.1 ppm. These three peaks have an integrated intensity ratio of 1:1:2 (Figure 2b). The downfield pair of peaks has a ^{19}F T_1 relaxation time of 3.7 s, while the upfield peak has a distinct ^{19}F T_1 of 10.7 s. Based on these intensities and T_1 values, we assign the two downfield peaks to one Phe residue and the upfield peak to the other Phe. Which peak corresponds to which Phe is obtained from the 3D correlation spectra shown below. At 7 kHz MAS, we observed high sideband intensities (Figure 2e,f), which were analyzed using the Herzfeld-Berger method[51] to give a ^{19}F anisotropy parameter of 58.1 and 59.4 ppm for the two Phe residues and 46.1 ppm for the Trp43. These values are near the rigid limit of ^{19}F chemical shift anisotropy (CSA),[52] indicating that these aromatic side chains are largely immobilized. The ^{19}F DP spectrum of F_4-TPP$^+$ bound to EmrE in the lipid membrane shows four peaks at isotropic chemical shifts of −96.5, −98.8, −100.6, and −101.4 ppm. This distribution indicates that the four chemically equivalent fluorines of the ligand are magnetically inequivalent due to their interactions with different protein side chains.[38]

The two CDN-labeled GB1 samples allowed us to test the ability of the 3D FNH experiment to assign fluorines based on their correlations with amide protons. We first conducted the 2D hNH-resolved ^{1}H−^{19}F REDOR experiment on the two GB1 samples. The REDOR difference (ΔS) spectrum between a control 2D spectrum (S_0) measured without ^{19}F pulses and a dephased spectrum (S) measured with the ^{19}F pulses yielded the signals of amide protons in close proximity to the fluorines. The difference spectrum of W-GB1 after 1.89 ms ^{1}H−^{19}F REDOR mixing (Figure 3a) shows G41, T53, V54, I6, and N8 signals, consistent with previous results.[21] In comparison, the REDOR difference spectrum of FF-GB1 (Figure 3b) shows a different set of peaks that chiefly involves residues in the N-terminal half of the protein. Resonance assignment using 3D hCANH (Figure 3d) indicates that FF-GB1 has slightly different ^{1}H and H^{N} chemical shifts from W-GB1 (Figure S2a,b).[53,54] For example, E27, T53, and V54 in FF-GB1 are perturbed compared to W-GB1, and Q2, T17, A24, T25, and A26 in FF-GB1 show peak splitting. Since the singly fluorinated W-GB1 has similar ^{1}H and ^{15}N chemical shifts as those of hydrogenated GB1,[33] the chemical shift changes of FF-GB1 might reflect a small degree of conformational perturbation due to the incorporation of two fluorines.

The different REDOR ΔS spectra between W-GB1 and FF-GB1 are not surprising. F30 lies near the N-terminus of the protein, surrounded by the first and second β-strands, and F52 points to the α-helix after the β2 strand (Figure 2d). In comparison, W43 resides on the β3 strand and is surrounded by residues in the C-terminal half of the protein. Thus, the three aromatic fluorines are surrounded by distinct residues, which should give rise to distinct REDOR difference spectra. For structurally unknown proteins, which fluorine atom causes dipolar dephasing to which H^{N} cannot be deduced from the REDOR difference spectra, and explicit correlation of the ^{19}F chemical shifts with the ^{1}H and/or ^{15}N chemical shifts is required.

To assign the fluorine-proximal H^{N} signals to each Phe side chain in the doubly fluorinated FF-GB1, we first conducted a 2D (F)NH version of the 3D OaB REDOR-CP FNH experiment. The omission of the ^{19}F chemical shift evolution allows us to evaluate the sensitivity and feasibility of this experiment. The 2D (F)NH correlation spectra of W-GB1 and FF-GB1 (Figure 3a,b), measured with a ^{1}H−^{19}F REDOR mixing time of 2 × 1.1 ms, show good agreement with the hNH-resolved REDOR difference spectra. All residues that exhibit S/S_0 values of less than 0.8 in the 1.89 ms hNH-resolved ^{1}H−^{19}F REDOR spectra exhibit cross peaks in the (F)NH spectrum. Those residues that have less substantial REDOR dephasing, such as I6 and L7 in FF-GB1, which have S/S_0 values greater than 0.9, do not show strong cross peaks in the 2D (F)NH spectra after 7 h of signal averaging. These 2D (F)NH correlation spectra were measured with twofold longer experimental time than the hNH-resolved REDOR difference spectra. But the signal-to-noise ratios (SNRs) of the (F)NH cross peaks are still two- to threefold lower than the REDOR difference spectra (Figure 3c). Thus, the 2D (F)NH experiment has 20−40% of the sensitivity of the hNH-resolved REDOR experiment (Figure 3c).

A 2D F(N)H experiment that correlates the ^{19}F and ^{1}H^{N} chemical shifts while omitting the ^{15}N chemical shift evolution is another approach for ^{19}F chemical shift assignment. The 2D F(N)H spectrum of FF-GB1 (Figure 4a) shows three ^{1}H cross peaks for the upfield ^{19}F signal at −111.1 ppm and two strong ^{1}H cross peaks for the downfield ^{19}F peak at −109.2 ppm. Comparison with the known H^{N} chemical shifts of GB1 allows us to assign the ^{1}H cross peaks in the −111.1 ppm cross

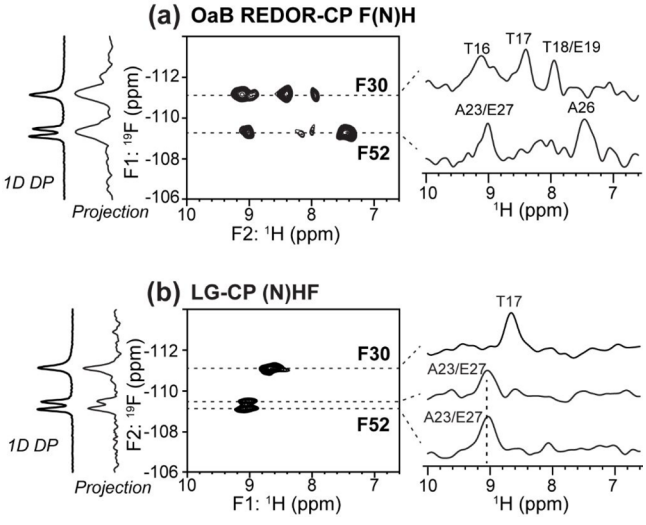

Figure 4. Comparison of 2D ^{19}F−^{1}H correlation spectra of FF-GB1 measured using the OaB REDOR-CP FNH experiment and the LG-CP NHF experiment. The spectra were measured under 38 kHz MAS. (a) 2D OaB REDOR-CP F(N)H spectrum measured using a ^{1}H−^{19}F REDOR mixing time of 2 × 1.1 ms. The ^{19}F peaks at −111.1 and −109.2 ppm can be assigned to F30 and F52, respectively, based on the H^{N} cross peaks. ^{1}H cross sections are shown on the right. (b) 2D LG-CP (N)HF spectrum, measured with a ^{1}H−^{19}F CP contact time of 1.4 ms. Note the two frequency dimensions are rotated from the spectrum in (a). Only one H^{N} cross peak is observed in each ^{19}F slice, indicating dipolar truncation of the weak ^{1}H−^{19}F couplings by the strong ^{1}H−^{19}F coupling.

https://doi.org/10.1021/acs.jpca.2c05154
J. Phys. Chem. A 2022, 126, 7021−7032

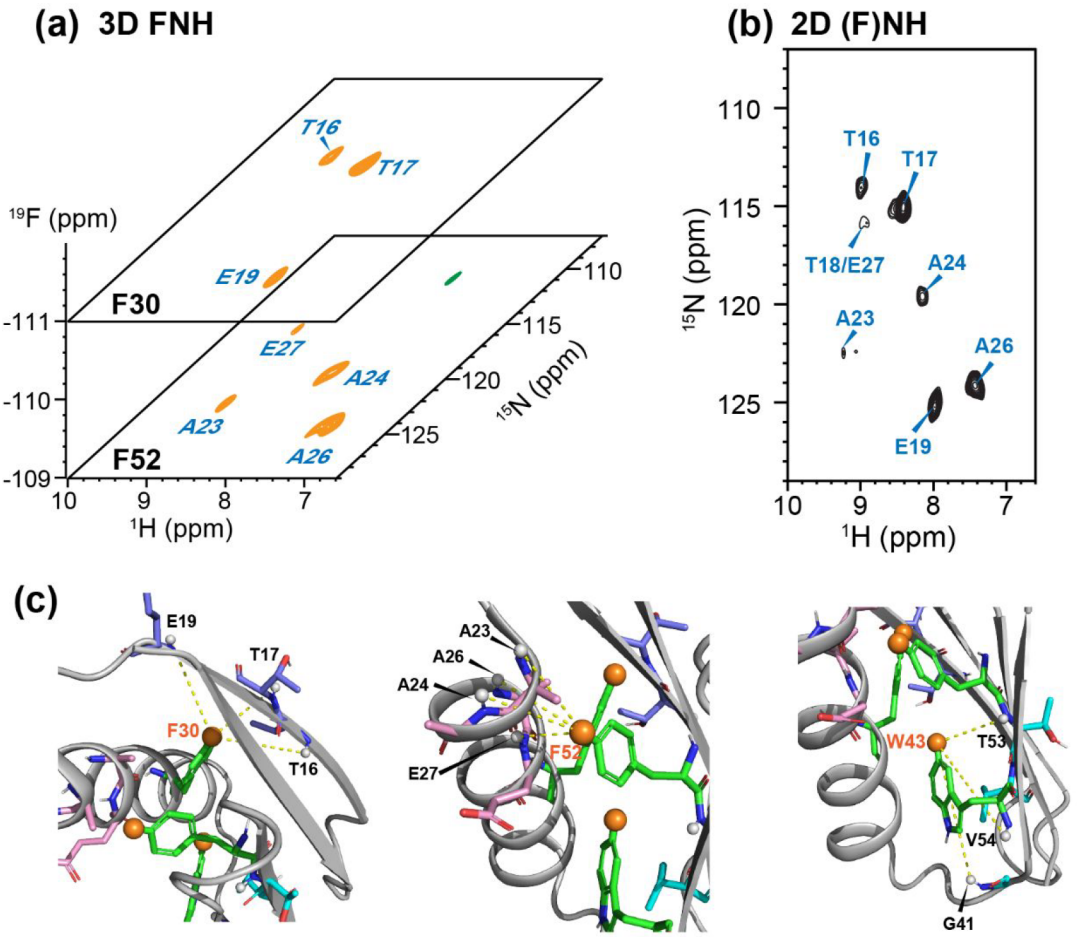

Figure 5. OaB REDOR-CP 3D FNH spectrum of FF-GB1 to demonstrate the resolution of H^N-F contacts. The spectra were measured under 38 kHz MAS. (a) 3D FNH spectrum, with the two 4-^{19}F Phe cross sections shown separately for F30 and F52. Resonance assignment was made based on the 2D F(N)H and (F)NH spectra. (b) 2D (F)NH spectrum, measured using a ^{1}H−^{19}F REDOR mixing time of 2 × 1.1 ms. (c) Crystal structure of GB1 (PDB: 2LGI). The residues whose amide protons are close to the two Phe residues and that are detected in the 3D FNH spectra are indicated. The residues closest to 5-^{19}F-Trp43 are identified by the 2D (F)NH spectrum in Figure 3b.

section to T16, T17 and T18 or E19, while the two ^{1}H signals in the −109.2 ppm ^{19}F cross section can be assigned to A23 or E27 and A26, respectively.

The 2D LG-CP (N)HF experiment is another way to correlate ^{19}F and H^N chemical shifts (Figure 4b). Using a ^{15}N−^{1}H LG-CP contact time of 0.8 ms and a ^{1}H−^{19}F CP contact time of 1.4 ms, we obtained a 2D spectrum that shows one main ^{1}H cross peak for each ^{19}F signal. The ^{1}H resonances in the −109.2 ppm ^{19}F cross section can be tentatively assigned to A23 and E27, while the ^{1}H cross peak in the −111.1 ppm cross section can be assigned to T17. Compared to the OaB REDOR-CP F(N)H spectrum, the LG-CP (N)HF spectrum shows only one ^{1}H cross peak for each ^{19}F. We attribute this difference to dipolar truncation of weak ^{1}H−^{19}F coupling by the strong ^{1}H−^{19}F dipolar coupling during the ^{1}H−^{19}F CP step.[55] In addition, spin diffusion between the amide protons and aromatic protons during ^{1}H−^{19}F CP could preferentially enhance the intensities of certain amide protons over others.

In addition to the different numbers of H^N-F cross peaks, the OaB REDOR-CP F(N)H experiment and LG-CP (N)HF experiment differ in the ^{1}H chemical shift resolution. The former gives high ^{1}H chemical shift resolution due to ^{1}H detection, while the sparse ^{19}F spectrum is encoded in the indirect dimension. The LG-CP (N)HF experiment detects the sparse ^{19}F spectrum while encoding the ^{1}H chemical shifts in the indirect dimension, thus giving inferior ^{1}H spectral resolution. For these reasons, we chose to conduct the 3D ^{19}F, ^{15}N, and ^{1}H correlation experiment using the OaB REDOR-CP pulse sequence.

Figure 5a shows the 3D OaB REDOR-CP FNH spectrum of FF-GB1, measured in 39 h. The ^{1}H−^{15}N plane for the −111.1 ppm ^{19}F peak exhibits T16, T17, and E19 cross peaks, whereas the −109.2 ppm ^{19}F cross section shows ^{1}H−^{15}N cross peaks for A23, A24, A26, and E27. The sum of the two cross sections matches the 2D (F)NH spectrum (Figure 5b), as expected. Based on the GB1 structure (Figure 5c), we can assign the −111.1 ppm ^{19}F peak to F30, whose Hξ atom, replaced by ^{19}F here, has short distances of 5.7−6.1 Å to the three amide protons resolved in the plane (Table 1). The −109.2 ppm peak can be assigned to F52, whose Hξ is 3.4−5.2 Å away from the four resolved H^N sites. Among these four amide protons, the close contact of E27 H^N to F52 Hξ had not been detected in the 2D (F)NH spectrum (Figure 5b), the F(N)H spectrum (Figure 4a), and ^{1}H−^{19}F REDOR difference spectrum (Figure 3a). Thus, 3D ^{19}F−^{1}H-^{15}N correlation allowed full resolution of the short distances between the fluorines and their neighboring amide protons. The 3.4 Å distance between F52 Hξ and E27 H^N is much shorter than the 5.0 Å distances

https://doi.org/10.1021/acs.jpca.2c05154
J. Phys. Chem. A 2022, 126, 7021−7032

Table 1. Distances between Hξ of the Two Phe Residues and Neighboring Amide Protons of GB1 (PDB: 2LGI)[a]

residue	Hξ F30	Hξ F52
T16 H^N	**6.5 Å**	12.1 Å
T17 H^N	**5.7 Å**	12.8 Å
E19 H^N	**6.1 Å**	11.2 Å
A23 H^N	10.1 Å	**5.1 Å**
A24 H^N	10.8 Å	**5.2 Å**
A26 H^N	7.3 Å	**4.9 Å**
E27 H^N	7.4 Å	**3.4 Å**

[a]The listed amide protons correspond to the signals observed in the ^{19}F, ^{1}H, and ^{15}N correlation spectra. Distances for observed 4-^{19}F–F30 to H^N and 4-^{19}F–F52 to H^N cross peaks are bolded.

between F52 Hξ and the three Ala amide protons. This suggests that the single H^N peak in the F52 ^{19}F cross section in the 2D LG-CP (N)HF spectrum (Figure 4b) may arise from E27.

3D OaB REDOR-CP FNH Experiment of F_4-TPP$^+$ Bound EmrE. With this demonstration of the 3D FNH experiment on GB1, we next applied the technique to the bacterial transporter EmrE. EmrE is a dimeric membrane protein that effluxes polyaromatic cationic substrates across the inner membrane of Gram-negative bacteria to cause multidrug resistance.[56−58] Substrate export against the concentration gradient is driven by coupling to proton import from the acidic periplasm to the neutral cytoplasm. Using $^{19}F-^{1}H$ REDOR NMR, we recently determined two high-resolution structures of EmrE bound to a tetrafluorinated substrate, F_4-TPP$^+$.[37,38] The two structures were solved at pH 5.8 and pH 8.0 to understand how the protonation state of the proton-selective residue E14 affects the substrate-bound structures of the protein.

Interestingly, although the ligand TPP$^+$ has tetrahedral symmetry around the central phosphorus, the four fluorines at the corners of the ligand are not structurally equivalent after binding. At both low and high pH, the 1D ^{19}F NMR spectra resolve multiple chemical shifts (Figure 2c). The high-pH

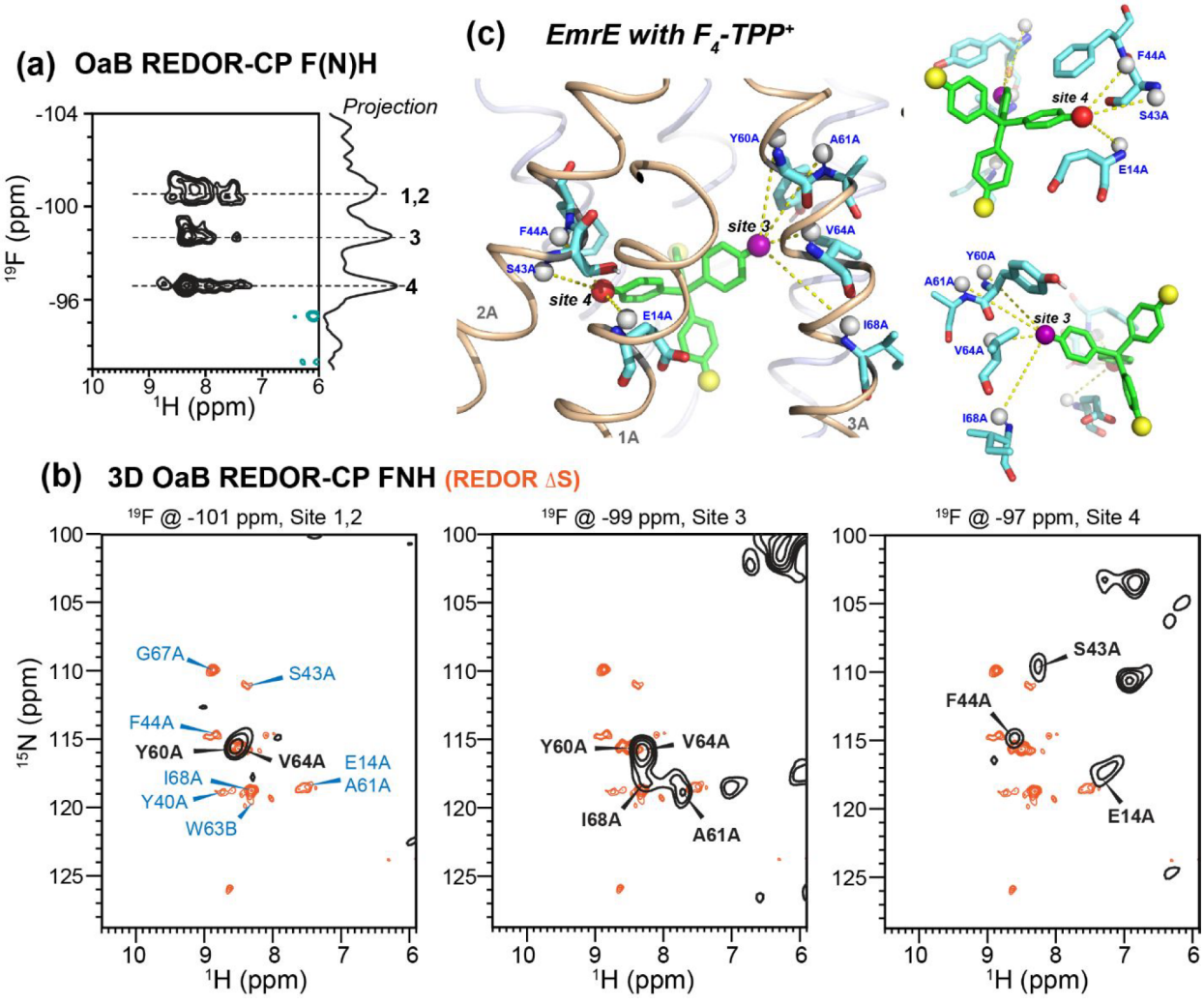

Figure 6. 2D and 3D OaB REDOR-CP FNH spectrum of F_4-TPP$^+$ complexed to EmrE at pH 8. (a) 2D F(N)H spectrum, measured under 38 kHz MAS using a $^{1}H-^{19}F$ REDOR mixing time of 2 × 1.1 ms. (b) 3D FNH spectrum of substrate-bound EmrE. Three cross sections at ^{19}F chemical shifts of −101, −99, and −97 ppm are shown. Assignment of the $^{1}H-^{15}N$ cross peaks is based on previously reported chemical shifts.[38] (c) Structure of F_4-TPP complexed EmrE in lipid bilayers at high pH. The four ligand fluorines are surrounded by different protein residues. Site-4 fluorine (red) is in close proximity to S43A, F44A, and E14A, while site-3 fluorine (magenta) is in close proximity to Y60A, V64A, A61A, and I68A. These are consistent with the $^{1}H-^{15}N$ cross peaks seen in the respective ^{19}F cross sections of the 3D spectrum.

https://doi.org/10.1021/acs.jpca.2c05154
J. Phys. Chem. A 2022, 126, 7021−7032

protein−substrate complex exhibits three resolved ^{19}F signals, numbered as 4 to 1 from the downfield to the upfield chemical shifts. This chemical shift distribution indicates that the four fluorines of the substrate experience different chemical and conformational environments, most likely due to their contact with different protein residues. Although we measured 2D hNH resolved ^{1}H−^{19}F REDOR difference spectra, without ^{19}F correlation to ^{1}H or ^{15}N chemical shifts, we did not directly assign which of the four fluorines caused dipolar dephasing to specific protein amide protons. Instead, the disambiguation of the short-distance ^{19}F−H^{N} spin pairs was carried out computationally during structure calculation.

The 3D OaB REDOR-CP FNH experiment allowed us to assign the ^{19}F peaks with respect to their neighboring protein amide protons. We first measured a 2D F(N)H spectrum to correlate the three resolved ^{19}F signals of the ligand with the H^{N} chemical shifts (Figure 6a). The most downfield ^{19}F peak at −97 ppm (site 4) has the narrowest line width and was previously shown to have the strongest ^{13}C−^{19}F dipolar coupling with the protein.[38] Consistently, the ^{19}F−^{1}H cross peak intensities are the highest for site 4, followed by site 3, the ^{19}F signal at −99 ppm. No ^{1}H assignment can be made from this 2D F(N)H spectrum due to substantial resonance overlap in the ^{1}H dimension. By introducing a ^{15}N chemical shift dimension, it became possible to resolve the amide protons that are correlated to the three fluorines. In the −97 ppm ^{19}F cross section for site 4, three ^{1}H−^{15}N cross peaks are resolved and can be assigned to S43A (of subunit A), F44A, and E14A (Figure 6b). In the −99 ppm ^{19}F cross section for site 3, we resolved four peaks that can be assigned to Y60A/V64A, A61A, and I68A. Inspection of the high-pH EmrE structural model (Figure 6c) indicates that the ^{19}F atom shown in red is in close proximity to the S43A (5.0 Å), F44A (4.5 Å), and E14A (5.2 Å) amide protons; thus, it can be assigned to site 4. The ^{19}F atom colored in magenta is in close proximity to V64A (4.0 Å), Y60A (6.9 Å), A61A (7.1 Å), and I68A (7.5 Å) and, thus, can be assigned to site 3.

DISCUSSION AND CONCLUSIONS

The 2D and 3D ^{19}F−^{1}H−^{15}N correlation spectra of GB1 (Figures 4 & 5) and EmrE (Figure 6) above demonstrate that the OaB REDOR-CP technique is effective for revealing which protein amides are close to which fluorine in a multifluorinated system. The correlation of the three frequency dimensions allows structurally based assignment in two contexts. First, if the ^{19}F chemical shifts of individual residues are already assigned based on mutagenesis and single-site fluorination,[59] then the FNH spectrum provides information about which fluorine is close to which amide protons in the hNH-resolved REDOR difference spectra. For structurally unknown proteins that contain *n* fluorines, the lack of ^{19}F correlation gives rise to an *n*-fold ambiguity, which is removed by the FNH correlation experiment. Second, if the ^{19}F chemical shift assignment is not known, which can occur for small molecules and when single-site fluorination of a protein is not possible, then the FNH correlation spectrum allows the association of each fluorine with its nearest amide protons. This grouping of all amide protons that are correlated with the same fluorine dramatically reduces ambiguity in the structure calculation.

It is of interest to compare the present OaB REDOR-CP FNH experiment with previously reported 2D and 3D correlation experiments that involve a ^{19}F dimension. 3D ^{19}F−^{1}H−^{1}H (FHH) and ^{19}F−^{19}F−^{1}H (FFH) experiments have been demonstrated on pharmaceutical compounds.[24,30] The ^{19}F−^{1}H correlations are established by CP, while the ^{1}H−^{1}H and ^{19}F−^{19}F correlations are established by radio-frequency-driven recoupling (RFDR) under ∼65 kHz MAS. These 3D experiments take advantage of the 100% natural abundance of ^{19}F and ^{1}H. However, they cannot be easily extended to macromolecules because the number of protons that need to be spectrally resolved is much larger than in small molecules even with protein perdeuteration. Therefore, multidimensional correlation involving another heteronuclear spin beside ^{1}H is necessary for spectral assignment and distance analysis.

Interestingly, the OaB REDOR pulse sequence was recently shown to have inferior efficiency and sensitivity compared to TEDOR sequences for ^{13}C−^{19}F correlation.[22] We attribute this opposite behavior of ^{13}C−^{19}F and ^{1}H−^{19}F correlation to the lack of ^{13}C spins in the fluorinated aromatic residues. ^{19}F T_1 and T_2 relaxation are well-known to be more rapid than for other nuclei due to its large CSA and strong couplings to protons. Thus, for ^{13}C−^{19}F correlation, the experiment that entails the least ^{19}F relaxation will have the highest sensitivity, while for ^{1}H−^{19}F correlation, the experiment that suffers the least dipolar truncation will outperform other experiments.

The 3D ^{19}F−^{15}N−^{1}H correlation technique demonstrated here is compatible with the commonly used 2D hNH experiment for measuring ^{1}H-detected solid-state NMR spectra under fast MAS. Since the 3D FNH correlation experiment has lower sensitivity than the 2D implementations, only relatively short ^{19}F−^{1}H REDOR mixing times should be used. This restricts the distance range that can be measured in the 3D experiment to less than 1 nm. However, the main purpose of the 3D experiment is to assign each fluorine to its spatially proximal amide hydrogens. Thus, we anticipate that a divide-and-conquer approach of conducting the 3D FNH experiment with short mixing times for resonance assignment and the 2D hNH-resolved ^{1}H−^{19}F REDOR experiments (Figure 1d) for measuring nanometer distances to be the most fruitful. The 3D FNH experiment is also complementary to ^{13}C−^{19}F correlation, which allows the use of conformation-dependent ^{13}C chemical shifts to resolve ^{19}F chemical shifts and ^{19}F-based distances. Therefore, these two experiments can be used in combination to measure nanometer distances between fluorinated ligands and their protein targets or between sparsely fluorinated aromatic side chains and backbone amide protons. Finally, the FNH experiment can be extended in two directions. First, ^{13}C instead of ^{15}N correlation can be implemented, giving an FCH experiment that should be useful for measuring distances to protein side chains. Second, the FNH or FCH experiment can be implemented on fully protonated samples by spinning at ∼100 kHz using 0.7 mm or smaller rotors. The use of protonated samples would simplify protein expression and purification, especially for challenging systems such as membrane proteins. Under ∼100 kHz MAS, we expect the ^{1}H−^{1}H dipolar couplings to not affect ^{1}H−^{19}F polarization transfer beyond a moderate change of the ^{1}H T_2 relaxation time. A 2D Hα-Cα correlation spectrum can be potentially sufficiently resolved to augment the 2D ^{1}H−^{15}N fingerprint to give site-resolved distance information. One potential drawback of faster MAS is that the ^{19}F refocusing pulses will take up a larger fraction of the rotor period. However, previous work on REDOR with finite pulses has shown that this is not a significant limitation.[21,60]

https://doi.org/10.1021/acs.jpca.2c05154
J. Phys. Chem. A 2022, 126, 7021−7032

■ ASSOCIATED CONTENT

Supporting Information

The Supporting Information is available free of charge at https://pubs.acs.org/doi/10.1021/acs.jpca.2c05154.

MALDI-MS and FPLC data of protein purification, additional NMR spectra, a table of NMR experimental conditions, and Bruker topspin pulse programs (PDF)

■ AUTHOR INFORMATION

Corresponding Author

Mei Hong − *Department of Chemistry, Massachusetts Institute of Technology, Cambridge, Massachusetts 02139, United States;* orcid.org/0000-0001-5255-5858; Email: meihong@mit.edu

Authors

Pu Duan − *Department of Chemistry, Massachusetts Institute of Technology, Cambridge, Massachusetts 02139, United States;* orcid.org/0000-0002-7395-4353

Aurelio J. Dregni − *Department of Chemistry, Massachusetts Institute of Technology, Cambridge, Massachusetts 02139, United States;* orcid.org/0000-0003-3422-4734

Complete contact information is available at: https://pubs.acs.org/10.1021/acs.jpca.2c05154

Notes

The authors declare no competing financial interest.

■ ACKNOWLEDGMENTS

This work is supported by NIH Grant No. GM088204 to M.H. and the P41 Grant No. GM132079 to the MIT-Harvard Center for Magnetic Resonance. The EmrE sample was produced by P. Spreacker in the Henzler-Wildman laboratory at the University of Wisconsin Madison.

■ REFERENCES

(1) de la Torre, B. G.; Albericio, F. The Pharmaceutical Industry in 2020. An Analysis of FDA Drug Approvals from the Perspective of Molecules. *Molecules* **2021**, *26*, 627.

(2) Zhou, Y.; Wang, J.; Gu, Z.; Wang, S.; Zhu, W.; Aceña, J. L.; Soloshonok, V. A.; Izawa, K.; Liu, H. Next Generation of Fluorine-Containing Pharmaceuticals, Compounds Currently in Phase II-III Clinical Trials of Major Pharmaceutical Companies: New Structural Trends and Therapeutic Areas. *Chem. Rev.* **2016**, *116*, 422−518.

(3) Hagmann, W. K. The many roles for fluorine in medicinal chemistry. *J. Med. Chem.* **2008**, *51*, 4359−69.

(4) Juweid, M. E.; Cheson, B. D. Positron-Emission Tomography and Assessment of Cancer Therapy. *N. Engl. J. Med.* **2006**, *354*, 496−507.

(5) Zeng, F.; Goodman, M. M. Fluorine-18 Radiolabeled Heterocycles as PET Tracers for Imaging β-Amyloid Plaques in Alzheimer's Disease. *Curr. Top. Med. Chem.* **2013**, *13*, 909−919.

(6) Villemagne, V. L.; Fodero-Tavoletti, M. T.; Masters, C. L.; Rowe, C. C. Tau imaging: early progress and future directions. *Lancet Neurol.* **2015**, *14*, 114−124.

(7) Shcherbakov, A. A.; Medeiros-Silva, J.; Tran, N.; Gelenter, M. D.; Hong, M. From Angstroms to Nanometers: Measuring Interatomic Distances by Solid-State NMR. *Chem. Rev.* **2022**, *122*, 9848−9879.

(8) Sharaf, N. G.; Gronenborn, A. M. (19)F-Modified Proteins and (19)F-Containing Ligands as Tools in Solution NMR Studies of Protein Interactions. *Methods Enzymol.* **2015**, *565*, 67−95.

(9) Didenko, T.; Liu, J. J.; Horst, R.; Stevens, R. C.; Wüthrich, K. Fluorine-19 NMR of integral membrane proteins illustrated with studies of GPCR. *Curr. Opin. Struct. Biol.* **2013**, *23*, 740−747.

(10) Klein-Seetharaman, J.; Getmanova, E. V.; Loewen, M. C.; Reeves, P. J.; Khorana, H. G. NMR spectroscopy in studies of light-induced structural changes in mammalian rhodopsin: Applicability of solution F-19 NMR. *Proc. Natl. Acad. Sci. U.S.A.* **1999**, *96*, 13744−13749.

(11) Kitevski-LeBlanc, J. L.; Prosser, R. S. Current applications of ^{19}F NMR to studies of protein structure and dynamics. *Prog. Nucl. Magn. Reson. Spectrosc.* **2012**, *62*, 1−33.

(12) Salwiczek, M.; Nyakatura, E. K.; Gerling, U. I. M.; Ye, S.; Koksch, B. Fluorinated Amino Acids: Compatibility with Native Protein Structures and Effects on Protein-Protein Interactions. *Chem. Soc. Rev.* **2012**, *41*, 2135−2171.

(13) Dürr, U. H.; Grage, S. L.; Witter, R.; Ulrich, A. S. Solid state ^{19}F NMR parameters of fluorine-labeled amino acids. Part I: Aromatic substituents. *J. Magn. Reson.* **2008**, *191*, 7−15.

(14) Grage, S. L.; Dürr, U. H.; Afonin, S.; Mikhailiuk, P. K.; Komarov, I. V.; Ulrich, A. S. Solid state F-19 NMR parameters of fluorine-labeled amino acids. Part II: Aliphatic substituents. *J. Magn. Reson.* **2008**, *191*, 16−2.

(15) Mehring, M.; Griffin, R. G.; Waugh, J. S. F-19 shielding tensors from coherently narrowed NMR powder spectra. *J. Chem. Phys.* **1971**, *55*, 746−755.

(16) Lu, M.; Sarkar, S.; Wang, M.; Kraus, J.; Fritz, M.; Quinn, C. M.; Bai, S.; Holmes, S. T.; Dybowski, C.; Yap, G. P. A.; et al. ^{19}F Magic Angle Spinning NMR Spectroscopy and Density Functional Theory Calculations of Fluorosubstituted Tryptophans: Integrating Experiment and Theory for Accurate Determination of Chemical Shift Tensors. *J. Phys. Chem. B* **2018**, *122*, 6148−6155.

(17) Kim, S. J.; Cegelski, L.; Preobrazhenskaya, M.; Schaefer, J. Structures of Staphylococcus aureus cell-wall complexes with vancomycin, eremomycin, and chloroeremomycin derivatives by ^{13}C{^{19}F} and ^{15}N{^{19}F} rotational-echo double resonance. *Biochemistry* **2006**, *45*, 5235−5250.

(18) Studelska, D. R.; Klug, C. A.; Beusen, D. D.; McDowell, L. M.; Schaefer, J. Long-range distance measurements of protein binding sites by rotational-echo double-resonance NMR. *J. Am. Chem. Soc.* **1996**, *118*, 5476−5477.

(19) Gullion, T.; Schaefer, J. Rotational-echo double-resonance NMR. *J. Magn. Reson.* **1989**, *81*, 196−200.

(20) Graesser, D. T.; Wylie, B. J.; Nieuwkoop, A. J.; Franks, W. T.; Rienstra, C. M. Long-range F-19-N-15 distance measurements in highly-C-13, N-15-enriched solid proteins with F-19-dephased REDOR shift (FRESH) spectroscopy. *Magn. Reson. Chem.* **2007**, *45*, S129−S134.

(21) Shcherbakov, A. A.; Hong, M. Rapid measurement of long-range distances in proteins by multidimensional 13C-19F REDOR NMR under fast magic-angle spinning. *J. Biomol. NMR* **2018**, *71*, 31−43.

(22) Shcherbakov, A. A.; Roos, M.; Kwon, B.; Hong, M. Two-dimensional (19)F-(13)C correlation NMR for (19)F resonance assignment of fluorinated proteins. *J. Biomol. NMR* **2020**, *74*, 193−204.

(23) Lu, M.; Wang, M.; Sergeyev, I. V.; Quinn, C. M.; Struppe, J.; Rosay, M.; Maas, W.; Gronenborn, A. M.; Polenova, T. ^{19}F Dynamic Nuclear Polarization at Fast Magic Angle Spinning for NMR of HIV-1 Capsid Protein Assemblies. *J. Am. Chem. Soc.* **2019**, *141*, 5681−5691.

(24) Lu, X.; Skomski, D.; Thompson, K. C.; McNevin, M. J.; Xu, W.; Su, Y. Three-Dimensional NMR Spectroscopy of Fluorinated Pharmaceutical Solids under Ultrafast Magic Angle Spinning. *Anal. Chem.* **2019**, *91*, 6217−6224.

(25) Roos, M.; Wang, T.; Shcherbakov, A. A.; Hong, M. Fast Magic-Angle-Spinning ^{19}F Spin Exchange NMR for Determining Nanometer ^{19}F-^{19}F Distances in Proteins and Pharmaceutical Compounds. *J. Phys. Chem. B* **2018**, *122*, 2900−2911.

(26) Wang, M.; Lu, M.; Fritz, M.; Quinn, C.; Byeon, I.-J.; Byeon, C.-H.; Struppe, J.; Maas, W.; Gronenborn, A.; Polenova, T. Fast Magic

Angle Spinning ^{19}F NMR of HIV-1 Capsid Protein Assemblies. *Angew. Chem., Int. Ed. Engl.* **2018**, *57*, 16375−16379.
(27) Lane Gilchrist, M.; Monde, K.; Tomita, Y.; Iwashita, T.; Nakanishi, K.; McDermott, A. E. Measurement of Interfluorine Distances in Solids. *J. Magn. Reson.* **2001**, *152*, 1−6.
(28) Roos, M.; Mandala, V. S.; Hong, M. Determination of Long-Range Distances by Fast Magic-Angle-Spinning Radiofrequency-Driven ^{19}F-^{19}F Dipolar Recoupling NMR. *J. Phys. Chem. B* **2018**, *122*, 9302−9313.
(29) Fritz, M.; Kraus, J.; Quinn, C. M.; Yap, G. P. A.; Struppe, J.; Sergeyev, I. V.; Gronenborn, A. M.; Polenova, T. Measurement of Accurate Interfluorine Distances in Crystalline Organic Solids: A High-Frequency Magic Angle Spinning NMR Approach. *J. Phys. Chem. B* **2019**, *123*, 10680−10690.
(30) Lu, X.; Huang, C.; Li, M.; Skomski, D.; Xu, W.; Yu, L.; Byrn, S. R.; Templeton, A. C.; Su, Y. Molecular Mechanism of Crystalline-to-Amorphous Conversion of Pharmaceutical Solids from (19)F Magic Angle Spinning NMR. *J. Phys. Chem. B* **2020**, *124*, 5271−5283.
(31) Lu, X.; Li, M.; Huang, C.; Lowinger, M. B.; Xu, W.; Yu, L.; Byrn, S. R.; Templeton, A. C.; Su, Y. Atomic-Level Drug Substance and Polymer Interaction in Posaconazole Amorphous Solid Dispersion from Solid-State NMR. *Mol. Pharmaceutics* **2020**, *17*, 2585−2598.
(32) Quinn, C. M.; Zadorozhnyi, R.; Struppe, J.; Sergeyev, I. V.; Gronenborn, A. M.; Polenova, T. Fast ^{19}F Magic-Angle Spinning Nuclear Magnetic Resonance for the Structural Characterization of Active Pharmaceutical Ingredients in Blockbuster Drugs. *Anal. Chem.* **2021**, *93*, 13029−13037.
(33) Shcherbakov, A. A.; Mandala, V. S.; Hong, M. High-Sensitivity Detection of Nanometer ^{1}H-^{19}F Distances for Protein Structure Determination by 1H-Detected Fast MAS NMR. *J. Phys. Chem. B* **2019**, *123*, 4387−4391.
(34) Mandala, V. S.; McKay, M. J.; Shcherbakov, A. A.; Dregni, A. J.; Kolocouris, A.; Hong, M. Structure and drug binding of the SARS-CoV-2 envelope protein transmembrane domain in lipid bilayers. *Nat. Struct. Mol. Biol.* **2020**, *27*, 1202−1208.
(35) Mandala, V. S.; Liao, S. Y.; Gelenter, M. D.; Hong, M. The Transmembrane Conformation of the Influenza B Virus M2 Protein in Lipid Bilayers. *Sci. Rep.* **2019**, *9*, 3725.
(36) Mandala, V. S.; Loftis, A. R.; Shcherbakov, A. A.; Pentelute, B. L.; Hong, M. Atomic Structures of Closed and Open Influenza B M2 Proton Channel Reveal the Conduction Mechanism. *Nat. Struc. Mol. Biol.* **2020**, *27*, 160−167.
(37) Shcherbakov, A. A.; Hisao, G.; Mandala, V. S.; Thomas, N. E.; Soltani, M.; Salter, E. A.; Davis, J. H.; Henzler-Wildman, K. A.; Hong, M. Structure and dynamics of the drug-bound bacterial transporter EmrE in lipid bilayers. *Nat. Commun.* **2021**, *12*, 172.
(38) Shcherbakov, A. A.; Spreacker, P. J.; Dregni, A. J.; Henzler-Wildman, K. A.; Hong, M. High-pH structure of EmrE reveals the mechanism of proton-coupled substrate transport. *Nat. Commun.* **2022**, *13*, 991.
(39) Duan, P.; Chen, K. J.; Wijegunawardena, G.; Dregni, A. J.; Wang, H. K.; Wu, H.; Hong, M. Binding Sites of a Positron Emission Tomography Imaging Agent in Alzheimer's β-Amyloid Fibrils Studied Using 19F Solid-State NMR. *J. Am. Chem. Soc.* **2022**, *144*, 1416−1430.
(40) Cai, M.; Huang, Y.; Yang, R.; Craigie, R.; Clore, G. M. A simple and robust protocol for high-yield expression of perdeuterated proteins in Escherichia coli grown in shaker flasks. *J. Biomol. NMR* **2016**, *66*, 85−91.
(41) Shi, X.; Rienstra, C. M. Site-Specific Internal Motions in GB1 Protein Microcrystals Revealed by 3D 2H-^{13}C-^{13}C Solid-State NMR Spectroscopy. *J. Am. Chem. Soc.* **2016**, *138*, 4105−4119.
(42) Böckmann, A.; Gardiennet, C.; Verel, R.; Hunkeler, A.; Loquet, A.; Pintacuda, G.; Emsley, L.; Meier, B. H.; Lesage, A. Characterization of different water pools in solid-state NMR protein samples. *J. Biomol. NMR* **2009**, *45*, 319−327.
(43) Hong, M.; Griffin, R. G. Resonance Assignment for Solid Peptides by Dipolar-Mediated ^{13}C/^{15}N Correlation Solid-State NMR. *J. Am. Chem. Soc.* **1998**, *120*, 7113−7114.
(44) Zhou, D. H.; Rienstra, C. M. High-performance solvent suppression for proton detected solid-state NMR. *J. Magn. Reson.* **2008**, *192*, 167−172.
(45) Gullion, T.; Schaefer, J. Elimination of resonance offset effects in rotational-echo double resonance NMR. *J. Magn. Reson.* **1991**, *92*, 439−442.
(46) Hing, A. W.; Vega, S.; Schaefer, J. Transferred-echo double-resonance NMR. *J. Magn. Reson.* **1992**, *96*, 205−209.
(47) Lee, M.; Goldburg, W. I. Nuclear-magnetic-resonance line narrowing by a rotating rf field. *Phys. Rev.* **1965**, *140*, A1261−A1271.
(48) Jaroniec, C. P.; Filip, C.; Griffin, R. G. 3D TEDOR NMR Experiments for the Simultaneous Measurement of Multiple Carbon-Nitrogen Distances in Uniformly ^{13}C,^{15}N-Labeled Solids. *J. Am. Chem. Soc.* **2002**, *124*, 10728−10742.
(49) Pan, Y.; Gullion, T.; Schaefer, J. Determination of C-N internuclear distances by rotational-echo double-resonance NMR of solids. *J. Magn. Reson.* **1990**, *90*, 330.
(50) Hong, M.; Yao, X. L.; Jakes, K.; Huster, D. Investigation of molecular motions by Lee-Goldburg cross-polarization NMR spectroscopy. *J. Phys. Chem. B* **2002**, *106*, 7355−7364.
(51) Herzfeld, J.; Berger, A. E. Sideband intensities in NMR spectra of samples spinning at the magic angle. *J. Chem. Phys.* **1980**, *73*, 6021.
(52) Duncan, T. M. *Principal Components of Chemical Shift Tensors: A Compilation,* 2nd ed.; The Farragut Press: Madison, WI, 1997.
(53) Andreas, L. B.; Jaudzems, K.; Stanek, J.; Lalli, D.; Bertarello, A.; Le Marchand, T. L.; Cala-De Paepe, D.; Kotelovica, S.; Akopjana, I.; Knott, B.; et al. Structure of fully protonated proteins by proton-detected magic- Angle spinning NMR. *Proc. Natl. Acad. Sci. U. S. A.* **2016**, *113*, 9187−9192.
(54) Zhou, D. H.; Shea, J. J.; Nieuwkoop, A. J.; Franks, W. T.; Wylie, B. J.; Mullen, C.; Sandoz, D.; Rienstra, C. M. Solid-state protein-structure determination with proton-detected triple-resonance 3D magic-angle-spinning NMR spectroscopy. *Angew. Chem., Int. Ed. Engl.* **2007**, *46*, 8380−8383.
(55) Bayro, M. J.; Huber, M.; Ramachandran, R.; Davenport, T. C.; Meier, B. H.; Ernst, M.; Griffin, R. G. Dipolar truncation effect in magic-angle spinning NMR recoupling experiments. *J. Chem. Phys.* **2009**, *130*, 114506.
(56) Morrison, E. A.; DeKoster, G. T.; Dutta, S.; Vafabakhsh, R.; Clarkson, M. W.; Bahl, A.; Kern, D.; Ha, T.; Henzler-Wildman, K. A. Antiparallel EmrE exports drugs by exchanging between asymmetric structures. *Nature* **2012**, *481*, 45−50.
(57) Chen, Y.-J.; Pornillos, O.; Lieu, S.; Ma, C.; Chen, A. P.; Chang, G. X-ray structure of EmrE supports dual topology model. *Proc. Natl. Acad. Sci. U. S. A.* **2007**, *104*, 18999.
(58) Schuldiner, S. EmrE, a model for studying evolution and mechanism of ion-coupled transporters. *Biochim. Biophys. Acta* **2009**, *1794*, 748−62.
(59) Frieden, C.; Hoeltzli, S. D.; Bann, J. G. The Preparation of ^{19}F-Labeled Proteins for NMR Studies. *Methods Enzym.* **2004**, *380*, 400−415.
(60) Jaroniec, C. P.; Tounge, B. A.; Rienstra, C. M.; Herzfeld, J.; Griffin, R. G. Recoupling of Heteronuclear Dipolar Interactions with Rotational-Echo Double-Resonance at High Magic-Angle Spinning Frequencies. *J. Magn. Reson.* **2000**, *146*, 132−139.

https://doi.org/10.1021/acs.jpca.2c05154
J. Phys. Chem. A 2022, 126, 7021−7032

Supporting Information

Solid-State NMR ^{19}F-^{1}H-^{15}N Correlation Experiments for Resonance Assignment and Distance Measurements of Multi-fluorinated Proteins

Pu Duan, Aurelio J. Dregni and Mei Hong *

Department of Chemistry, Massachusetts Institute of Technology, 170 Albany Street, Cambridge, MA 02139

* Corresponding author: Professor Mei Hong, meihong@mit.edu

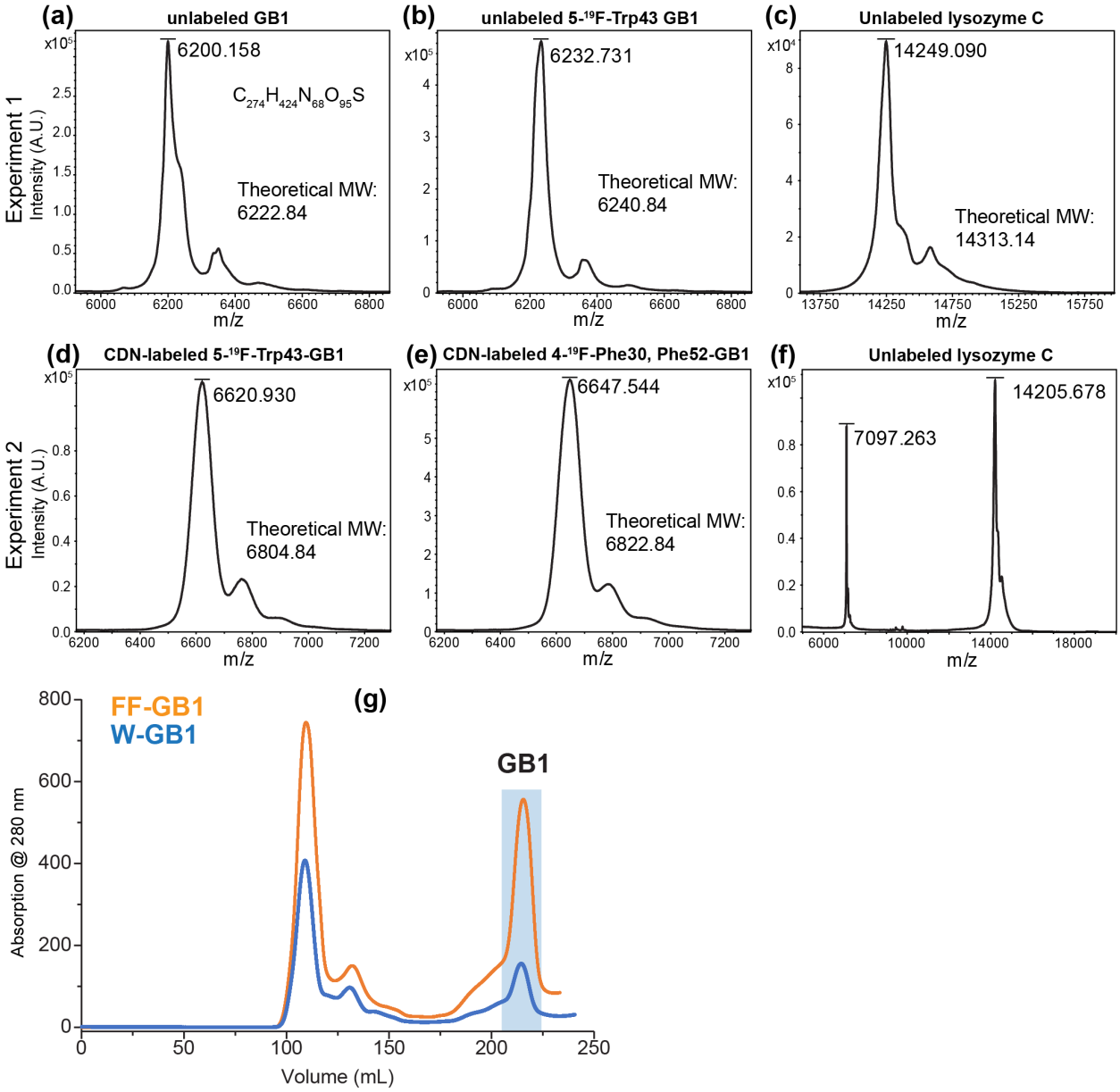

Figure S1. MALDI-TOF mass spectra and FPLC size exclusion chromatograms of the fluorinated GB1 samples used in this study. Mass spectra of lysozyme are additionally measured as a reference. (**a**) Natural abundance GB1. (**b**) 5-^{19}F-Trp labeled GB1. (**c**) Natural abundance lysozyme. (**d**) CDN-labeled and 5-^{19}F-Trp labeled GB1. (**e**) CDN-labeled and 4-^{19}F-Phe30, Phe52 labeled GB1. (**f**) Natural abundance lysozyme C. Spectra in (**a-c**) were measured in the same run and spectra (**d-e**) were measured together in another run. All measured peak maxima are slightly below the theoretical molecular weight, as manifested by the reference spectrum of lysozyme. The molecular weight difference between CDN-GB1 and natural abundance GB1 qualitatively matches the ^{13}C, ^{15}N and ^{2}H labels introduced into the protein. (**g**) FPLC chromatograms of W-GB1 and FF-GB1. Elution from 208 min to 225 min was collected.

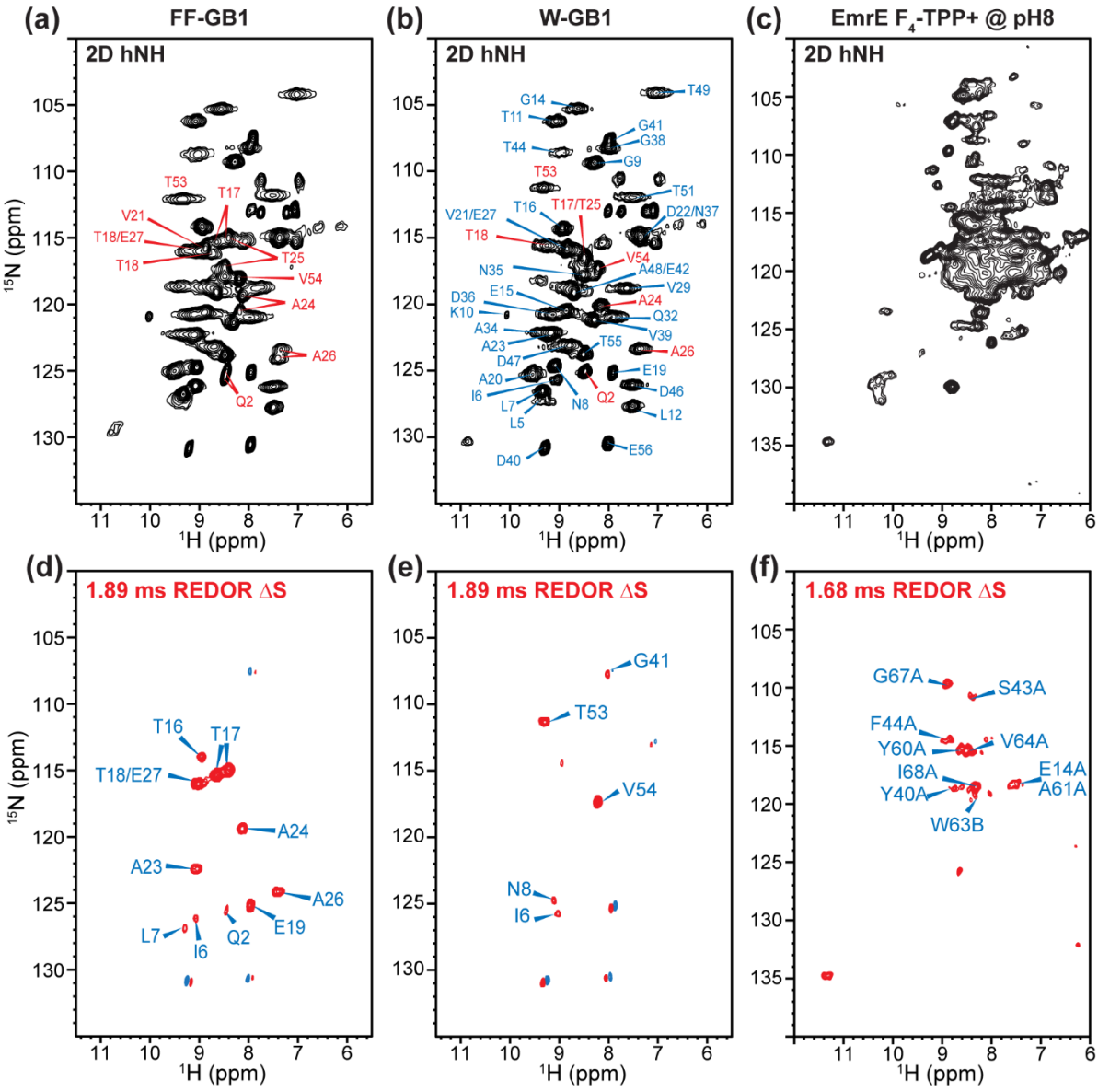

Figure S2. 2D hNH spectra (a-c) and hNH-resolved ^{1}H-^{19}F REDOR difference (ΔS) spectra (d-f) of GB1 and EmrE. (**a, d**) Spectra of FF-GB1. Chemical shifts are assigned using the 3D hCANH experiment, and the residues with different chemical shift from W-GB1 are annotated in red. (**b, e**) Spectra of W-GB1. ^{1}H and ^{15}N chemical shifts were obtained from the literature [29]. Those residues annotated in panel (a) are also highlighted in red. (**c, f**) Spectra of substrate bound EmrE. Chemical shift assignment was carried over from a recent study [33].

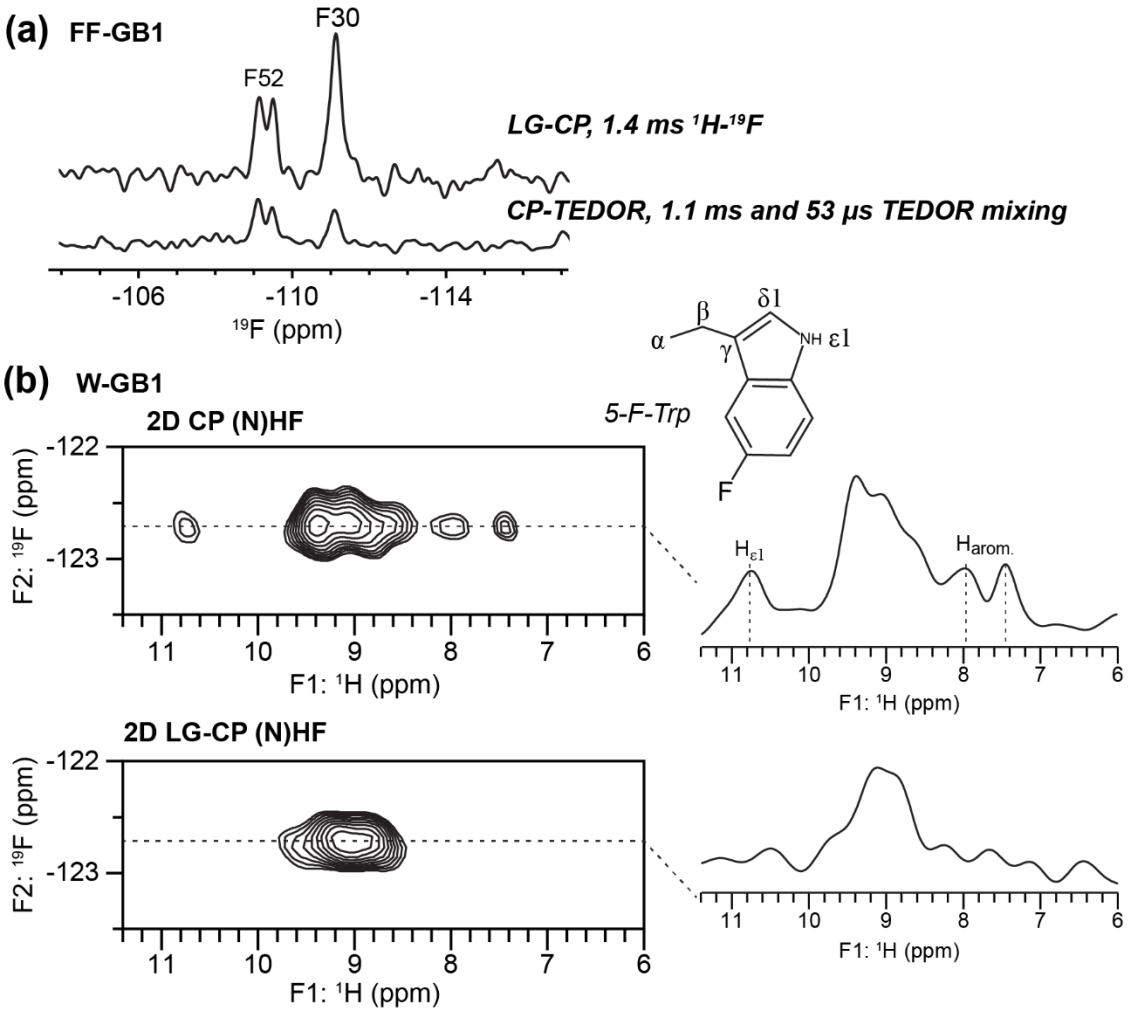

Figure S3. Additional spectra to compare the efficiencies of the various ^{19}F-^{1}H-^{15}N correlation experiments. (**a**) 1D ^{19}F-detected LG-CP (NH)F spectrum of FF-GB1 measured with 1.4 ms ^{1}H-^{19}F CP contact time, compared with the 1D CP-TEDOR (NH)F spectrum measured using a first TEDOR mixing time of 1.1 ms and a second TEDOR mixing time of 53 µs. The two spectra are scaled by the number of scans. (**b**) 2D CP and LG-CP (N)HF spectra of W-GB1, and the 1D cross section at -122.7 ppm ^{19}F chemical shift. Hε1 and two other aromatic protons of 5-^{19}F-Trp are observed in the CP (N)HF spectrum, which are absent in the LG-CP (N)HF spectrum.

Table S1. Detailed conditions of the solid-state NMR experiments in this study.

Sample	Experiment	Experimental Parameters	Experimental Time
CDN 4-^{19}F-F30/F52 GB1	1D ^{19}F DP	ν_{MAS} = 7 kHz, ns = 256, τ_{rd} = 25 s, τ_{dw} = 2.5 μs, τ_{acq} = 10.2 ms.	1.8 hr
	1D ^{19}F DP	ν_{MAS} = 38 kHz, ns = 256, τ_{rd} = 25 s, τ_{dw} = 2.5 μs, τ_{acq} = 10.2 ms.	1.8 hr
	1D ^{19}F LG-CP (NH)F	ns = 256, τ_{rd} = 1.7 s, τ_{dw} = 2.5 μs, τ_{acq} = 10.24 ms, τ_{HN} = 1.4 ms, τ_{NH} = 0.8 ms, τ_{HF} = 1.4 ms, $\nu_{1H,LG}$ = 71.4 kHz	7 min
	1D ^{19}F CP-TEDOR (NH)F	ns = 1024, τ_{rd} = 1.7 s, τ_{dw} = 2.5 μs, τ_{acq} = 10.24 ms, τ_{HN} = 1.4 ms, τ_{NH} = 0.8 ms, $\tau_{19F,180}$ = 6.8 μs, $\tau_{TEDOR,1}$ = 1.1 ms, $\tau_{TEDOR,2}$ = 53 or 110 μs, $\nu_{1H,LG}$ = 71.4 kHz	29 min each
	2D hNH	ns = 8, τ_{rd} = 1.7 s, $t_{1,max}$ = 30 ms, $t_{1,inc}$ = 250 μs, τ_{dw} = 25 μs, τ_{acq} = 30 ms, τ_{HN} = 1 ms, τ_{NH} = 0.8 ms, $\tau_{MISSISSIPPI}$ = 0.2 s. WDW = QSINE 3	1 hr
	2D hNH detected ^{1}H-^{19}F REDOR	ns = 16, τ_{rd} = 1.7 s, $t_{1,max}$ = 30 ms, $t_{1,inc}$ = 250 μs, τ_{dw} = 25 μs, τ_{acq} = 30 ms, τ_{HN} = 1 ms, τ_{NH} = 0.6 ms, $\tau_{MISSISSIPPI}$ = 0.2 s, $\tau_{19F,180}$ = 6.8 μs, τ_{REDOR} = 1.9, 3.8, 5.7, 7.6 ms. WDW = QSINE 3	2 hr each for S and S_0, 4×4 hr total.
	2D OaB REDOR-CP F(N)H	ns = 176, τ_{rd} = 1.7 s, $t_{1,max}$ = 2.5 ms, $t_{1,inc}$ = 52.6 μs, τ_{dw} = 25 μs, τ_{acq} = 30 ms, τ_{HN} = 1 ms, τ_{NH} = 0.6 ms, $\tau_{MISSISSIPPI}$ = 0.2 s, $\tau_{19F,180}$ = 6.8 μs, τ_{REDOR} = 2×1.1 ms. WDW = GM, LB = -15 Hz, GB = 0.05.	8 hr
	2D OaB REDOR-CP (F)NH	ns = 192, τ_{rd} = 1.7 s, $t_{1,max}$ = 10 ms, $t_{1,inc}$ = 250 μs, τ_{dw} = 25 μs, τ_{acq} = 30 ms, τ_{HN} = 1 ms, τ_{NH} = 0.6 ms, $\tau_{MISSISSIPPI}$ = 0.2 s, $\tau_{19F,180}$ = 6.8 μs, τ_{REDOR} = 2×1.1 ms. WDW = GM, LB = -15 Hz, GB = 0.07. Linear prediction in F1.	7 hr
	2D LG-CP (N)HF	ns = 160, τ_{rd} = 1.7 s, $t_{1,max}$ = 12.5 ms, $t_{1,inc}$ = 250 μs, τ_{dw} = 2.5 μs, τ_{acq} = 10.24 ms, τ_{HN} = 1.4 ms, τ_{NH} = 0.8 ms, τ_{HF} = 1.4 ms, $\nu_{1H,LG}$ = 71.4 kHz, WDW = GM, LB = -15 Hz, GB = 0.05.	8 hr
1.3 mm HXY probe	3D hCaNH	ns = 8, τ_{rd} = 1.4 s, $t_{1,max}$ = 4.5 ms, $t_{1,inc}$ = 160 μs, $t_{2,max}$ = 11.1 ms, $t_{1,inc}$ = 300 μs, τ_{dw} = 10 μs, τ_{acq} = 25 ms, τ_{HC} = 1.5 ms, τ_{CN} = 10 ms, τ_{NH} = 0.8 ms, $\nu_{1HspecificCP}$ = 7 kHz, $\tau_{MISSISSIPPI}$ = 0.15 s. WDW = QSINE 3. Linear prediction in F1 and F2.	14 hr
	3D OaB REDOR-CP FNH	ns = 16, τ_{rd} = 1.7 s, $t_{1,max}$ = 2.5 ms, $t_{1,inc}$ = 52.6 μs, $t_{2,max}$ = 10 ms, $t_{1,inc}$ = 250 μs, τ_{dw} = 25 μs, τ_{acq} = 30 ms, τ_{HN} = 1 ms, τ_{NH} = 0.6 ms, $\tau_{MISSISSIPPI}$ = 0.2 s, $\tau_{19F,180}$ = 6.8 μs, τ_{TEDOR} = 2×1.1 ms. WDW = GM, LB = -15 Hz, GB = 0.05.	39 hr
CDN 5-^{19}F-W43 GB1	1D ^{19}F DP	ν_{MAS} = 7 kHz, ns = 512, τ_{rd} = 5.5 s, τ_{dw} = 2.5 μs, τ_{acq} = 10.2 ms.	0.8 hr
	1D ^{19}F DP	ν_{MAS} = 38 kHz, ns = 512, τ_{rd} = 5.5 s, τ_{dw} = 2.5 μs, τ_{acq} = 10.2 ms.	0.8 hr

	2D hNH	ns = 8, τ_{rd} = 1.7 s, $t_{1,max}$ = 30 ms, $t_{1,inc}$ = 250 μs, τ_{dw} = 25 μs, τ_{acq} = 30 ms, τ_{HN} = 1 ms, τ_{NH} = 0.8 ms, $\tau_{MISSISSIPPI}$ = 0.2 s. WDW = QSINE 3	1 hr
	2D hNH detected ^{1}H-^{19}F REDOR	ns = 16, τ_{rd} = 1.7 s, $t_{1,max}$ = 30 ms, $t_{1,inc}$ = 250 μs, τ_{dw} = 25 μs, τ_{acq} = 30 ms, τ_{HN} = 1 ms, τ_{NH} = 0.6 ms, $\tau_{MISSISSIPPI}$ = 0.2 s, $\tau_{19F,180}$ = 6.8 μs, τ_{REDOR} = 1.9, 3.8, 5.7, 7.6 ms. WDW = QSINE 3.	2 hr each for S and S_0, 4×4 hr total.
	2D CP (N)HF	ns = 1024, τ_{rd} = 1.7 s, $t_{1,max}$ = 3 ms, $t_{1,inc}$ = 250 μs, τ_{dw} = 2.5 μs, τ_{acq} = 10.24 ms, τ_{HN} = 1.3 ms, τ_{NH} = 0.6 ms, τ_{HF} = 5 ms, WDW = GM, LB = -20 Hz, GB = 0.05 for F2, LB = -15 Hz, GB = 0.07 and linear predicted for F1.	11.6 hr
	2D LG-CP (N)HF	ns = 320, τ_{rd} = 1.7 s, $t_{1,max}$ = 3 ms, $t_{1,inc}$ = 100 μs, τ_{dw} = 2.5 μs, τ_{acq} = 10.24 ms, τ_{HN} = 1.3 ms, τ_{NH} = 0.7 ms, τ_{HF} = 5 ms, $\nu_{1H,LG}$ = 71.4 kHz, WDW = GM, LB = -20 Hz, GB = 0.05 for F2, LB = -15 Hz, GB = 0.07 and linear predicted for F1.	9.1 hr
	2D OaB REDOR-CP (F)NH	ns = 192, τ_{rd} = 1.7 s, $t_{1,max}$ = 10 ms, $t_{1,inc}$ = 250 μs, τ_{dw} = 25 μs, τ_{acq} = 30 ms, τ_{HN} = 1 ms, τ_{NH} = 0.6 ms, $\tau_{MISSISSIPPI}$ = 0.2 s, $\tau_{19F,180}$ = 6.8 μs, τ_{REDOR} = 2×0.95 ms. WDW = GM, LB = -15 Hz, GB = 0.07. Linear prediction in F1.	8 hr
CDN EmrE-TPP at pH 8.0	1D ^{19}F DP	ν_{MAS} = 38 kHz, ns = 512, τ_{rd} = 2 s, τ_{dw} = 2.5 μs, τ_{acq} = 10.2 ms.	20 min
	2D hNH	ns = 8, τ_{rd} = 1.7 s, $t_{1,max}$ = 30 ms, $t_{1,inc}$ = 300 μs, τ_{dw} = 10 μs, τ_{acq} = 25 ms, τ_{HN} = 1 ms, τ_{NH} = 0.7 ms, $\tau_{MISSISSIPPI}$ = 0.2 s. WDW = QSINE 3	1 hr
	2D hNH detected ^{1}H-^{19}F REDOR	ns = 16, τ_{rd} = 1.7 s, $t_{1,max}$ = 30 ms, $t_{1,inc}$ = 300 μs, τ_{dw} = 10 μs, τ_{acq} = 25 ms, τ_{HN} = 1 ms, τ_{NH} = 0.7 ms, $\tau_{MISSISSIPPI}$ = 0.2 s, $\tau_{19F,180}$ = 6.8 μs, τ_{REDOR} = 1.68 ms. WDW = QSINE 3.	1.7 hr each for S and S_0, 3.4 hr total.
	2D OaB REDOR-CP F(N)H	ns = 1136, τ_{rd} = 1.5 s, $t_{1,max}$ = 2.5 ms, $t_{1,inc}$ = 52.6 μs, τ_{dw} = 10 μs, τ_{acq} = 25 ms, τ_{HN} = 1 ms, τ_{NH} = 0.7 ms, $\tau_{MISSISSIPPI}$ = 0.3 s, $\tau_{19F,180}$ = 6.8 μs, τ_{REDOR} = 2×1.1 ms. WDW = GM, LB = -15 Hz, GB = 0.07.	54 hr
	3D OaB REDOR-CP FNH	ns = 48, τ_{rd} = 1.6 s, $t_{1,max}$ = 2.5 ms, $t_{1,inc}$ = 52.6 μs, $t_{2,max}$ = 10 ms, $t_{1,inc}$ = 250 μs, τ_{dw} = 10 μs, τ_{acq} = 25 ms, τ_{HN} = 1 ms, τ_{NH} = 0.7 ms, $\tau_{MISSISSIPPI}$ = 0.3 s, $\tau_{19F,180}$ = 6.8 μs, τ_{REDOR} = 2×1.1 ms. WDW = GM, LB = -40 Hz, GB = 0.02 for F3; LB = -20 Hz, GB = 0.05 for F2; LB = -20 Hz, GB = 0.03 for F1.	130 hr

*: unless specified, the MAS frequencies are 38 kHz for the 1.9 mm rotor experiments and 55 kHz for the 1.3 mm rotor experiments.

Symbols: NMR probe (rotor diameter, channels); ns = number of scans (transients) per free induction decay (FID); τ_{rd} = recycle delay between scans; $t_{1,max}$ = maximum t_1 (indirect dimension 1) evolution time; $t_{1,inc}$ = increment for t_1 (indirect dimension 1) evolution time; $t_{2,max}$ = maximum t_2 (indirect dimension 2) evolution time; $t_{2,inc}$ = increment for t_2 (indirect dimension 2) evolution time; τ_{dw} = dwell time during direct FID acquisition; τ_{acq} = maximum acquisition time during direct FID detection; τ_{XY} = cross polarization (CP) contact time during CP *from* channel X *to* channel Y;

$\nu_{1H,LG}$ = ^{1}H *rf* strength during LG CP; $\nu_{1HspecificCP}$ = ^{1}H dipolar decoupling field strength during heteronuclear CP; $\tau_{19F,180}$ = ^{19}F 180° pulse duration in ^{1}H-^{19}F REDOR and TEDOR; τ_{REDOR} = duration of REDOR recoupling time; $\tau_{TEDOR,1}$ = duration of the first TEDOR recoupling time; $\tau_{TEDOR,2}$ = duration of the second TEDOR recoupling time.

Pulse sequence for the OaB REDOR-CP FNH experiment.

```
;FNH_OaB_redorCP.pd
;FNH 3D based on Out-and-Back REDOR FH and hNH CP

;1D, 2D & 3D 19F-15N-1H experiment
;FH Out-and-Back REDOR, HN CP, NH CP, and H-detection

;Avance III version
;Parameters:
;f1 : H
;f2 : N
;f3 : F
;o1 : H offset, center of 1H signal
;o2 : N offset, center of 15N signal (~119 ppm)
;o3 : F offset, center of 19F signal
;p1 : F 90 hard pulse at pl3
;p2 : F 180 hard pulse at pl3
;p3 : H 90 hard pulse at pl1
;p4 : H 180 hard pulse at pl1
;p21 : N 90 hard pulse at pl2
;p22 : N 180 hard pulse at pl2
;p25 : HN CP at sp42 (H) & sp43 (N), (~1 ms)
;p45 : NH CP at sp46 (H) & sp47 (N), (~400 to 800 us)
;pl1 : H hard pulse power
;pl2 : N hard pulse power
;pl3 : F Hard pulse power
;pl12 : H dec power ('waltz16' @ ~7-10 kHz)
;pl13 : H dec power during H2O suppression (~15 kHz, 'cwX_13nofq', 'cwY_13nofq')
;pl16 : N dec power ('waltz16_16nofq' at ~7-10 kHz)
;sp42 : H HN CP power
;sp43 : N HN CP power
;sp46 : H NH CP power
;sp47 : N NH CP power
;d0 : incremented delay (t1)
;d1 : recycle delay; 1 to 5 times T1H
;d10: incremented delay (t2)
;d15: REDOR mixing time, ~1ms for 5A, need optimization
;d19 : delay for water suppression (~100 to 300 ms)
;cpdprg1 : H dec ('waltz16' at pl12 (~7-10 kHz))
;cpdprg2 : N dec ('waltz16_16nofq' at pl16 (~7-10 kHz))
;cpdprg4 : H Water suppression along X ('cwX_13nofq' at pl13 (15 kHz))
;cpdprg5 : H Water suppression along Y ('cwY_13nofq' at pl13 (15 kHz))
;pcpd1 : H dec pulse: 25-35.71 us ('waltz16' at ~7-10kHz)
;pcpd2 : N dec pulse: 25-35.71 us ('waltz16_16nofq' at ~7-10kHz)
;spnam42 : H shape (e.g. 'square.1000' for HN CP (=no shape))
;spnam43 : N shape (ramp up for HN CP, e.g. 'ramp.70100.1000')
;spnam46 : H shape (e.g. 'square.1000' for NH CP (=no shape))
;spnam47 : N shape (ramp down for NH CP, e.g. 'ramp.10070.1000')
;cnst31 : MAS frequency, kHz
;inf1 :  1/SW(F) = 2 * DW(F)
;inf2 :  1/SW(N) = 2 * DW(N)
;in0 : = inf1
;in10 : = inf2
;l0 : loopcounter for F1
;l10 : loopcounter for F2
```

```
;l1 : loop counter for REDOR, odd
;ZGOPTNS : -Dlacq : acquisition times > 50ms
;         or blank
;FnMODE : States-TPPI
;ns : 16


prosol relations=<biosolHCN>

#include <trigg.incl>
       ; definition of external trigger output

"acqt0=-1u"     ; baseopt correction

"spoff42=0.0"               ;############################
"spoff43=0.0"               ;#     ensure correct     #
"spoff46=0.0"               ;#     shape offsets      #
"spoff47=0.0"               ;############################

"d24=0.00025s/cnst31-p1/2"
"d25=0.00025s/cnst31-p3/2"
"d26=0.00025s/cnst31-p2/2"
"d27=0.00025s/cnst31-p4/2"
"d28=0.00025s/cnst31"

"p22=p21*2"
"p4=p3*2"

"d15=(l1+1)*0.001s/cnst31"

"in0=inf1"                  ;############################
"d0=1u"                     ;#     t1_init => 0, 0    #
"l0=0"                     ;############################

"in10=inf2"                 ;############################
"d10=1u"                    ;#     t2_init => 0, 0    #
"l10=0"                    ;############################

define delay ONTIME
                    ;############################
;$EXTERN                    ;# python insertion point #
                    ;############################

"ONTIME=aq+d0+p25+p45+d19"

Prepare, ze

;#########################################################
;#              Protections: Pre-Check               #
;#########################################################

#ifdef lacq
#else
#include <acq_prot.incl>
       ;Max. 50 ms acquisition time
#include <ONTIME_H_prot.incl>
```

```
      ;total RF deposition restriction to < 1 s
#endif                /* end of lacq */

#include <p25bio_prot.incl>
      ;p25 max. 10 ms
#include <p45bio_prot.incl>
      ;p45 max. 10 ms
#include <noH2Obio_prot.incl>
      ;water suppression d19 max. 500 ms

;------------Start of Active Pulse Program-------------

Start, 30m  do:f2

  d1  do:f1
  d15
  trigg

if "l10>0"
{
  "d52=d10-1u"
}

  (p3 pl1 ph1):f1
; ---------- H-F REDOR to generate HyFz --------------------
  d25 pl3:f3

4 d26:f3 ph7
  (p2 ph7^):f3
  d26
 lo to 4 times l1

  d27:f1 ph9
  (p4 ph9):f1
  d27

5 d26:f3 ph7
  (p2 ph7^):f3
  d26
 lo to 5 times l1

  d24
  (center (p3 ph11):f1 (p1 ph12):f3 ) ;90 pulses on X and Y
;--------------------- t1, evolving HzFy--------------------------
  d0   ;19F t1 evol.
; ---------- F-H REDOR, convert back to Hx --------------------
  (center (p3 ph13):f1 (p1 ph14):f3 ) ;90 pulses on X and Y
  d24 pl3:f3

6 d26:f3 ph8
  (p2 ph8^):f3
  d26
 lo to 6 times l1

  d27:f1 ph10
  (p4 ph10):f1
```

```
  d27

7 d26:f3 ph8
  (p2 ph8^):f3
  d26
 lo to 7 times l1

  d28

;--------------------- H-N CP --------------------------
  (p25:sp42 ph0):f1  (p25:sp43 ph2):f2

;--------- t2 evolution, Polarization on 15N-----------
  0.5u pl12:f1

if "l10>0"
{
  1u cpds1:f1                    ;cpds1 = waltz without power level
  d52
  1u do:f1  pl13:f1
}

;--------------Water suppression-----------------------

  (p21 pl2 ph3):f2          ; brings magn. to z

  0.5u cpds4:f1
  d19*0.25
  0.5u do:f1

  0.5u cpds5:f1
  d19*0.25
  0.5u do:f1

  0.5u cpds4:f1
  d19*0.25
  0.5u do:f1

  0.5u cpds5:f1
  d19*0.25
  0.5u do:f1

  (p21 pl2 ph4):f2          ; brings magn. to y

;----------------------N-H CP--------------------------

  (p45:sp47 ph5):f2  (p45:sp46 ph6):f1

;--------------------Aquisition-------------------------
  1u cpds2:f2

  gosc ph31     ;start ADC with ph31 signal routing

  1m do:f2

lo to Start times ns
```

```
30m mc #0 to Start
F1PH(calph(ph14, -90), caldel(d0, +in0) & calclc(l0, 1))
F2PH(calph(ph2, +90), caldel(d10, +in10) & calclc(l10, 1))

HaltAcqu, 1m
exit


ph1 = 1 3                ; H 90 hard pulse
ph0 = 0                  ; H HN CP Spin lock
ph2 = 1                  ; N HN CP Spin lock
ph3 = 0                  ; N 1st 90 hard pulse (flip to z)
ph4 = 0 0 0 0 2 2 2 2    ; N 2nd 90 hard pulse (flip back)
ph5 = 1                  ; N NH CP Spin lock
ph6 = 1                  ; H NH CP Spin lock

ph7 = 0 1 0 1 1 0 1 0    ; REDOR1 xy-16
      2 3 2 3 3 2 3 2
ph8 = 0 1 0 1 1 0 1 0    ; REDOR2 xy-16
      2 3 2 3 3 2 3 2

ph9 = 0                  ; REDOR1 180
ph10 = 0                 ; REDOR2 180
ph11 = 0 0 0 0 0 0 0 0   ; H flip up
       2 2 2 2 2 2 2 2
ph12 = 0                 ; F flip down
ph13 = 2                 ; H flip down
ph14 = 2 2 0 0           ; F flip up

ph31= 1 3 3 1 3 1 1 3
      3 1 1 3 1 3 3 1
```

Pulse sequence for the LG-CP NHF experiment.

```
;NHF_lgcp.pd
;NHF 3D based on NH LGCP and HF CP

;1D, 2D and 3D 15N-1H-19F CP experiment
;HN CP, NH CP, HF CP and F-detection

;Avance III version
;Parameters:

;f1 : F channel
;f2 : H channel
;f3 : N channel
;p1 : F 90 hard pulse at pl11
;p2 : F 180 hard pulse at pl11
;p3 : H 90 hard pulse at pl2
;p21 : N 90 hard pulse at pl21
;p22 : N 180 hard pulse at pl21
;p25 : HN CP at sp42 (H) & sp43 (N), (~1 to 3 ms)
;p45 : NH LGCP at pl46 (H) & sp47 (N), (~800 us)
;p15 : HF CP at sp48 (H) & sp49 (F)
;pl1 : F CP pulse power
;pl2 : H hard pulse power
;pl3 : not used
;pl11: F hard pulse power
;pl12 : H dec power ('waltz' at ~7-10 kHz)
;pl13 : H NH CP power preset
;pl16 : N dec power ('waltz16_16nofq' at 7-10 kHz)
;pl18 : F dec power ('waltz18_18nofq' at 7-10 kHz)
;pl21 : N hard pulse power
;pl22 : H HF CP power preset
;sp42 : H HN CP power
;sp43 : N HN CP power
;pl46 : H NH LGCP power
;sp47 : N NH CP power
;sp48 : H HF CP power
;sp49 : F HF CP power
;cnst16: base 1H frq
;cnst31: MAS frq in kHz
;d0 : incremented delay (t1)
;d1 : recycle delay; 1 to 5 times T1
;d10: incremented delay (t2)
;cpdprg1 : H dec ('waltz16' at pl12 (7-10 kHz))
;cpdprg2 : N dec ('waltz16_16nofq' at pl16 (7-10 kHz))
;cpdprg3 : F dec ('waltz16_18nofq' at pl18 (7-10 kHz))
;pcpd1 : H dec pulse: 25-35.71 us ('waltz16' at 7-10kHz)
;pcpd2 : N dec pulse: 25-35.71 us ('waltz16_16nofq' 7-10 kHz)
;pcpd3 : C dec pulse: 25-35.71 us ('waltz16_18nofq' 7-10 kHz)
;spnam42 : H shape (e.g. 'square.1000' for HN CP (=no shape))
;spnam43 : N shape (ramp up for HN CP, e.g. 'ramp.70100.1000')
;spnam47 : N shape (ramp down for NH CP, e.g. 'ramp.70100.1000')
;spnam48 : H shape ('square.1000' for HF CP (=no shape))
;spnam49 : F shape (ramp up for HF CP, e.g. 'ramp.80100.1000'e.g. )

;inf1 :  1/SW(N) = 2 * DW(N)
```

```
;inf2 :  1/SW(H) = 2 * DW(H)
;in0 : = inf1
;in10 : = inf2
;l0 : loopcounter for F1
;l10 : loopcounter for F2
;ZGOPTNS : -Dlacq : acquisition times > 50ms
;         or blank
;FnMODE : States-TPPI
;ns : 8
;ds : 2 or 4

prosol relations=<biosolHCN>


#include <trigg.incl>
       ; definition of external trigger output
#include <lgcalc.incl>       ; definition of Lee-Goldberg offsets

define pulse pma
"pma=p3*(3526/9000)"        ;calculate magic angle pulse based on 1H 90

"acqt0=-1u"                 ; baseopt correction

"spoff42=0.0"               ;############################
"spoff43=0.0"               ;#     ensure correct     #
"spoff47=0.0"               ;#     shape offsets      #
"spoff48=0.0"               ;#                        #
"spoff49=0.0"               ;############################

"p2=p1*2"
"p22=p21*2"
"cnst16=0"

"in0=inf1"                  ;############################
"d0=1u"                     ;#    t1_init => 0, 0     #
"in10=inf2"                 ;############################
"d10=1u"                    ;#    t2_init => 0, 0     #
"l0=0"                     ;############################
"l10=0"                     ;############################


                          ;############################
;$EXTERN                          ;# python insertion point #
                          ;############################


Prepare, ze

;### Protection check

#ifdef lacq
#else
#include <acq_prot.incl>
       ;Max. 50 ms acquisition time
#endif                /* end of lacq */
```

```
#include <noH2Obio_prot.incl>
       ;water suppression d19 max. 500 ms

;### Start

Start, 30m  do:f1 do:f2 do:f3

  d1
 (1u fq=cnst16):f2
  trigg

if "l0>0"
{
  "d51=d0-1u"
}

if "l10>0"
{
 "d52=d10-1u"
}

;----- H-N CP ------

  (p3 pl2 ph1):f2
  (p25:sp42 ph0):f2  (p25:sp43 ph2):f3

;---- 15N t1 evolution -------------
  0.25u pl12:f2

if "l0>0"
{
  0.5u cpds1:f2
  d51
  0.5u do:f2  pl13:f2
}
  0.25u fq=cnst23:f2
;----------- N-H CP-----------------
  (p45:sp47 ph5):f3  (p45 pl46 ph6):f2
  0.1u fq=0:f2
  (pma pl2 ph8):f2

;-----1H CS evolution t2------------------
  0.5u pl18:f3

if "l10>0"
{
  0.5u cpds3:f3
  d52
  0.5u do:f3
}

;---- H-F CP----------------

  (p15:sp49 ph7):f1    (p15:sp48 ph16):f2

  1u cpds1:f2 pl12:f2                    ;pl12 is used here with waltz
```

```
  gosc ph31     ;start ADC with ph31 signal routing

  1m do:f2
  1m do:f3

lo to Start times ns

30m mc #0 to Start
F1PH(calph(ph2, +90), caldel(d0, +in0) & calclc(l0, 1))
F2PH(calph(ph6, +90), caldel(d10, +in10) & calclc(l10, 1))

HaltAcqu, 1m
exit


ph1 = 1 3               ; H 90 hard pulse
ph0 = 0                 ; H HN CP Spin lock
ph2 = 1                 ; N HN CP Spin lock
ph5 = 1 1 3 3           ; N NH CP Spin lock
ph6 = 1                 ; H NH CP Spin lock
ph7 = 1                 ; F HF CP Spin lock
ph8 = 0                 ; H back to xy plane
ph16 = 1 1 1 1  3 3 3 3   ; H HF CP Spin lock
ph31 = 1 3 3 1  3 1 1 3   ; receiver
```